Proxemy Research Technical Report #V00-005

Author: Dr. Lori S. Glaze

Title: Final Report: 'Volcanic Plumes on Venus and Io'

Submitted to: Dr. John Grant/COTR
Code SR
NASA Headquarters

April 30, 2000

7335 Hanover Pkwy Suite C • Greenbelt, MD 20770 • (301) 313-0024 • E-mail: lori@proxemy.com

Proxemy Research is under contract to NASA to perform science research of volcanic plumes on Venus and Io. The following report constitutes delivery of ***Milestone Event #24*** under NASA contract NASW-98012.

TITLE: Final Report: 'Volcanic Plumes on Venus and Io', **PRI Tech. Rep. # V00-005.**

AUTHOR: Dr. Lori S. Glaze

1. Introduction

Since funding for this project began in April 1998, we have successfully completed all of the milestones set out in contract NASW-98012. The project covered by this contract is comprised of two distinct tasks that were outlined in the original proposal entitled " Volcanic plumes on Venus and Io," dated May 29, 1997. The first objective was to produce a manuscript that presents results from previous work funded by the NASA Planetary Geology and Geophysics Venus Data Analysis program. A reprint of the resulting manuscript "Transport of SO_2 by explosive volcanism on Venus" is submitted with this final report and composes Appendix A. The work leading up to this publication was described in the 1999 Annual Report PRI Technical Report #V99-005, included here as Appendix B.

The second objective was to develop a model that constrains stochastic-ballistic effects of variable ejection velocities on areal concentrations of volcanic deposits on Io. Much of the work over the last year has focused on this work. A copy of a manuscript accepted for publication in the Journal of Geophysical Research/Planets is included as Appendix C.

2. Summary of Milestone Events 1 - 12

The first year of this project was very productive. Task 1 of the originally proposed work was completed and significant progress was made on Task 2. Under Task 1, a manuscript describing the transport of SO_2 on Venus via convecting volcanic plumes was prepared, submitted, revised and accepted for publication (Appendix A contains a reprint). This study showed that explosive volcanism is still a plausible mechanism for SO_2 transport to the top of Venus' troposphere. Under Task 2, a stochastic-ballistic model for volcanic eruptions on Io was developed to address problems that surround mechanisms for creating annular deposits. Preliminary results for a variety of simple energy and angular distributions were able to generate annuli with dimensions similar to those seen at Prometheus (Galileo image #6578r). A detailed summary of the activities directed toward Milestone Events 1 - 12 was submitted in the first annual report for this project (PRI Technical Report #V99-005) and is included here as Appendix B (without appendices).

3. Summary of Milestone Events 13, 14 and 15

Activities directed toward Milestone Events #13, #14 and #15 focused on completing final revisions and reviewing proofs of the manuscript accepted for publication in JGR/Planets that described buoyant volcanic plume on Venus.

Work on Task 2 was begun in earnest during the time period covered by Milestone Events #13, #14 and #15. Time was spent applying the stochastic-ballistic emplacement model to a variety of possible eruption conditions on Io, including Maxwellian energy distributions and anisotropic ejection angle distributions. In addition, a significant proportion of hours was spent reviewing proposals for the Planetary Geology and Geophysics review panel.

4. Summary of Milestone Event 16

Minimal activity was reported on this project for Milestone Event #16.

5. Summary of Milestone Events 17 and 18

After completion of the Venus manuscript, efforts were begun on the preparation of a manuscript describing the stochastic-ballistic model. The initial draft manuscript developed under Milestone Event #17 explored three applications of the model that resulted in the formation of high particle concentration annuli surrounding a central source. The manuscript discussed the basic model for the single energy case, two distributed energy cases (Gaussian and Maxwellian), as well as a case with variable angular distributions. Results showed that the Maxwellian energy and some distributions of ejection angles can result in annuli with dimensions similar to that observed at Prometheus.

Activities directed toward Milestone Event #18 resulted in additional progress toward the preparation of a manuscript describing the stochastic-ballistic model. The necessity of equal binning (the same number of bins) of ejection angles, θ, and the range parameter, r, was explored. Time was spent looking in detail at where particles ejected at different angles end up on the ground. A variety of bin sizes were examined. For the Io annuli of interest, the radii are generally greater than 30 pixels (or 'bins') from the source. After this careful examination, it was determined that for most of the Io cases of interest, it is not necessary to further constrain the model. Some time was also spent generating publication quality figures for the manuscript.

6. Summary of Milestone Events 19 and 20

Activities associated with Milestone Events #19 and #20 were directed toward final preparation and submission of the manuscript describing the Stochastic-Ballistic emplacement model for eruptions on Io. Significant progress to this end was made in this time period when attention was directed in four primary areas:

1) furthering our understanding of the effects on ground concentrations resulting from truncation

of an isotropic angular distribution.

2) preparing and presenting a talk at the East Coast Volcanologists meeting at CEPS.

3) developing a new angular formulation for the stochastic ballistic model as opposed to the momentum formulation used previously.

4) incorporating the new conclusions drawn from (1) and (3), as well as feedback from the ECV meeting into the manuscript.

A brief summary of the model and results is given here. Figure 1 shows the effects of truncating the ejection cone for a single energy eruption on Io. The objective is to determine under what conditions an annulus of high particle concentrations on the ground can be generated. From Figure 1a, we can see that for isotropic ejection at all angles between 0 and 90°, there is a very strong peak in particle concentrations near the vent. This is due entirely to particles ejected at angles near 90°. This is a direct result of both the isotropic constraint that requires a equal number of particles per unit area pass through an imaginary hemisphere near the vent and a singularity in the formulation for ejection angles equal to 90°.

By truncating the ejection cone at 75° (Figure 1b) we not only eliminate the peak near the vent, but we simultaneously increase the relative magnitude of the peak near the maximum deposition distance. Figures 1c and 1d show what happens when the ejection cone is truncated at 45° and 20°, respectively.

Our conclusion after looking at the surface concentrations generated by simple ejection cone truncation is that if a little bit of noise were introduced into the energy distribution, we should be able to generate a broad peak of high particle concentrations at some distance from the vent.

Figure 2 shows the effects of both ejection cone truncation and the assumption of a normally distributed energy with RSD's ranging from 1 - 8%. For isotropic ejection to 90° (Figure 2a), we see that it is impossible to generate an annulus. For small RSD%, there is a small relative maximum near the maximum deposition distance, but a slight increase in the RSD results in an overall exponential decrease in particle concentrations.

Figure 2a illustrates the results for the ejection cone limited between 0 and 75° for normally distributed energies. All of these cases show a broad peak between 20 and 40 distance units from the vent. These dimensions are very similar to those observed at Prometheus in recent Galileo images. The shape of the surface distribution varies from slightly skewed to symmetric. The results of this study were presented at the ECV meeting in November.

Following the ECV meeting, some effort was directed toward an alternative approach to the Stochastic-ballistic model. The new approach uses an angular formulation as opposed to the momentum approach used prior to Milestone Event #19. The result is a direct formula for calculating the areal concentration of particles on the surface:

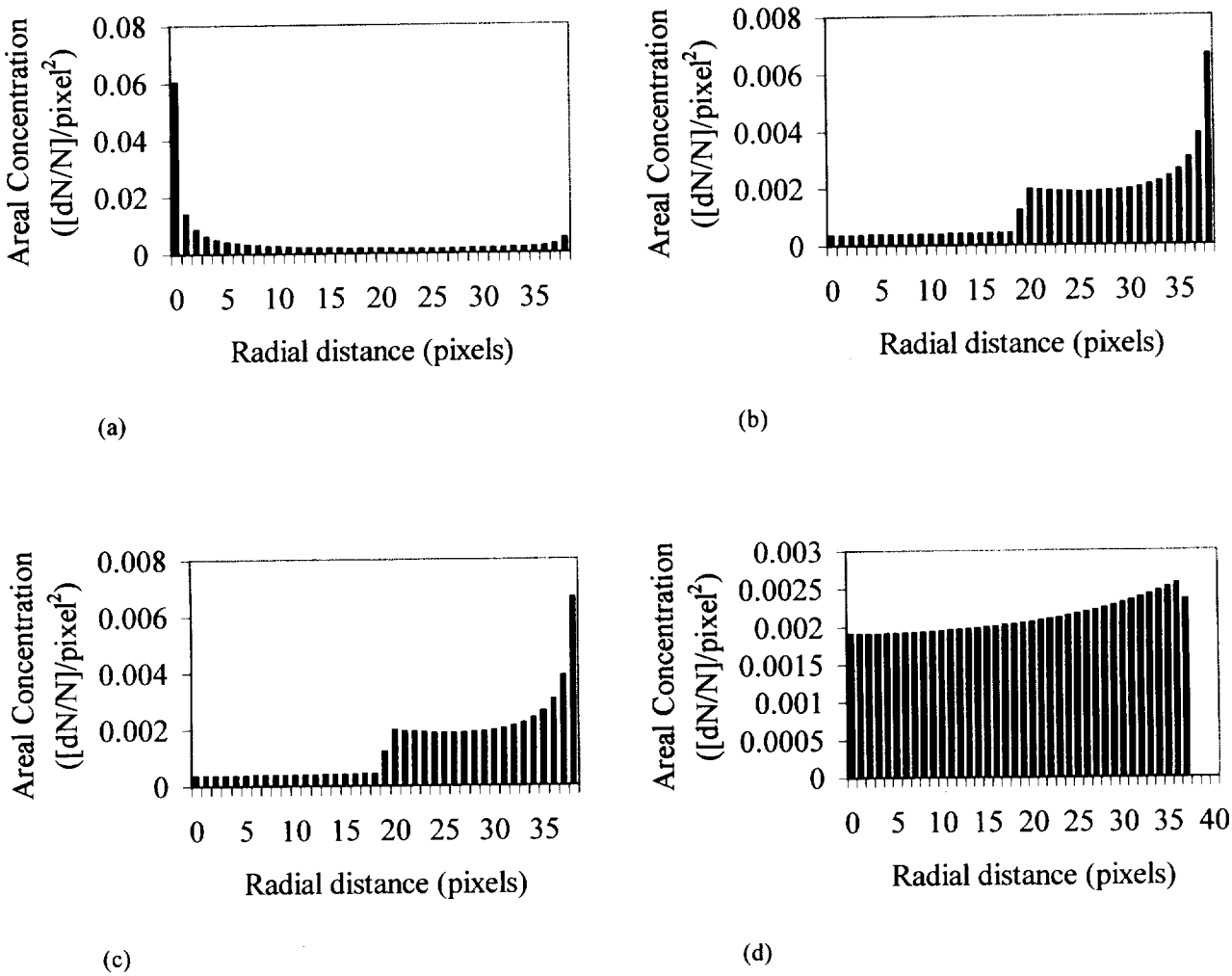
Areal Concentration ([dN/N]/pixel²)
0.08
0.06
0.04
0.02
0
0 5 10 15 20 25 30 35
Radial distance (pixels)
(a)
Areal Concentration ([dN/N]/pixel²)
0.008
0.006
0.004
0.002
0
0 5 10 15 20 25 30 35
Radial distance (pixels)
(b)
Areal Concentration ([dN/N]/pixel²)
0.008
0.006
0.004
0.002
0
0 5 10 15 20 25 30 35
Radial distance (pixels)
(c)
Areal Concentration ([dN/N]/pixel²)
0.003
0.0025
0.002
0.0015
0.001
0.0005
0
0 5 10 15 20 25 30 35 40
Radial distance (pixels)
(d)

Figure 1

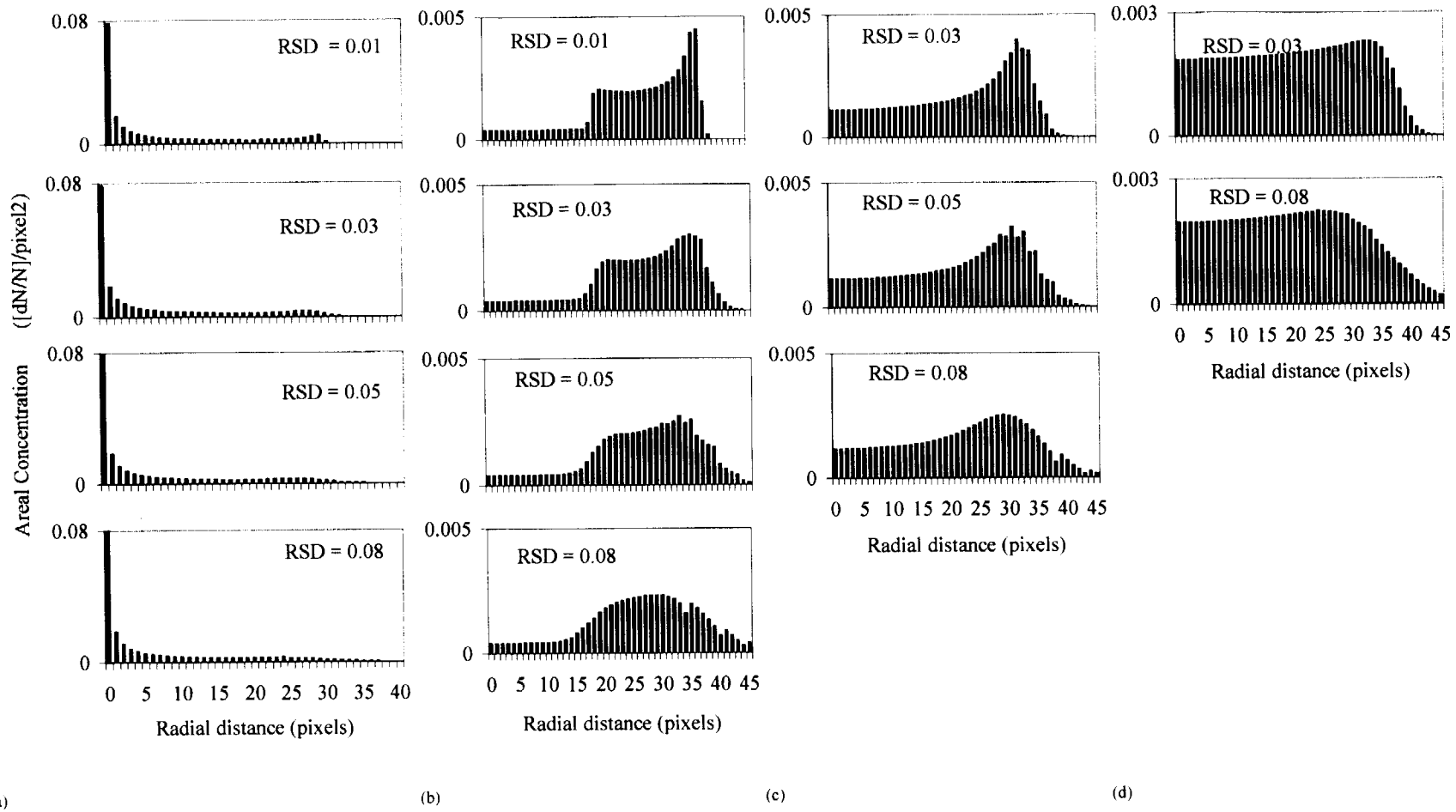
Areal Concentration ([dN/N]/pixel2)
RSD = 0.01
RSD = 0.03
RSD = 0.05
RSD = 0.08
0.08
0.005
0.003
0
0 5 10 15 20 25 30 35 40 45
Radial distance (pixels)
(a)
(b)
(c)
(d)

Figure 2

$$\rho(r) = \frac{1}{2\pi r}\frac{1}{N}\frac{dN}{dr} = \frac{1}{1-cos\theta_o}\frac{1}{4\pi r}\sqrt{\frac{1\pm\xi}{2}}\frac{1}{\xi r_{max}} \quad \textbf{(1)}$$

where

$$\xi = \sqrt{1-(r/r_{max})^2} \quad \textbf{(2)}$$

and r_{max} is the maximum deposition distance occurring when $v_r = v_z$:

$$r_{max} = \frac{v_o^2}{g} \quad \textbf{(3)}$$

All of the results discussed above were incorporated into the manuscript that was submitted in December 1999, completing Milestone Event #20. The manuscript, to appear in JGR-Planets, is included as Appendix C.

7. Summary of Milestone Event 21

Minimal activity was reported on this project for Milestone Event #21.

8. Summary of Milestone Event 22

Activities directed toward Milestone Event 22 were focused on putting together slides for a presentation at the Lunar and Planetary Science Conference to be held in March, 2000. The topic of the talk was stochastic-ballistic plumes on Io. The presentation discussed the results of the manuscript submitted under Milestone Event #20.

9. Summary of Milestone Event 23

Activities associated with Milestone Event #23 focused on attendance at the Lunar and Planetary Science Conference held in Houston. In addition to attending many interesting talks and posters, a talk was given entitled 'Stochastic-ballistic plumes on Io'. The presentation discussed results of the similarly titled manuscript included as Appendix C. The abstract for the LPSC presentation is included here as Appendix D.

Also as part of Milestone Event #23, reviews of the above referenced manuscript were received from the Journal of Geophysical Research/Planets. The editor indicated that the manuscript was accepted pending some minor revisions. Additional time was spent completing those revisions.

10. Summary of Milestone Event 24

Activities associated with Milestone Event #24 included the return of the Io manuscript to JGR/Planets, completion of this final report, and the preparation of a progress report for the NASA Planetary Geology and Geophysics Program. The final form of the manuscript is included here as Appendix C, and is officially 'in press' at the conclusion of Milestone Event #24.

11. Conclusions

This two year project has been extremely productive. In the first year, Task 1 of the originally proposed work was completed and significant progress was made on Task 2. Under Task 1, a manuscript describing the transport of SO_2 on Venus via convecting volcanic plumes was prepared, submitted, revised and accepted for publication. This study showed that explosive volcanism is still a plausible mechanism for SO_2 transport to the top of Venus' troposphere. In the second year, significant progress was made on Task 2, resulting in a manuscript describing a stochastic-ballistic model for volcanic eruptions on Io that was prepared, submitted, revised and accepted for publication. The model addresses problems that surround mechanisms for creating annular deposits. Results for a normal energy distribution and an isotropic angular distribution within an ejection cone (with a maximum ejection angle less than 90°) has been shown to generate annuli with dimensions similar to those seen at Prometheus (Galileo image #6578r).

APPENDIX A:

Transport of SO_2 by explosive volcanic plumes on Venus

JOURNAL OF GEOPHYSICAL RESEARCH, VOL. 104, NO. E8, PAGES 18,899–18,906, AUGUST 25, 1999

Transport of SO_2 by explosive volcanism on Venus

Lori S. Glaze

Proxemy Research, NASA Goddard Space Flight Center, Greenbelt, Maryland

Abstract. Observations by the Pioneer Venus orbiter and many different types of analyses have suggested the possibility of contemporary explosive volcanism on Venus. The rise of volcanic eruption plumes on Venus is reexamined using recent improvements in buoyant plume modeling. The first-order model applied to Venus by previous authors features nonphysical discontinuous solutions for all of the model parameters and lacks internal consistency in the formulation of the governing equations. This makes it difficult to assess the validity of the Venus applications and conclusions derived from these models. The model used here contains several improvements including two corrections to the formulation and a change in the criterion for the transition of the plume from the jet region to the buoyancy-driven region. The model used in earlier works assumed a discontinuous transition between these two regions, resulting in an overestimate of the transition height as well as the maximum plume height. The effect of the transition criterion is magnified on Venus, where the continuous solution appears to have very little dependence on initial vent size. In contrast, the discontinuous solution shows a very strong dependence on initial vent size. The continuous solution used here indicates that plumes on Venus become dominated by buoyancy effects almost immediately above the vent. Use of the discontinuous solution, however, suggests that jets up to 10 km above the vent are possible for the boundary conditions considered. The combined effect of using the older model for conditions on Venus is a 5–8% overestimate of the maximum plume height for vent radii ranging from 20 to 250 m. The influence of latitude and elevation are also explored. For large eruptions on Venus, plumes rising in the Northern Highlands would rise much higher than plumes with identical boundary conditions erupted in the equatorial Lowlands. This is due to the greater stability of the upper atmosphere at higher latitudes and the sharp decrease in atmospheric pressure as a function of altitude. To examine the net effect of all the model assumptions and ambient influences, eruptions are simulated for a range of conditions at Maat Mons and compared with results in the literature. These simulations indicate that for small mass fluxes, the new model predicts smaller plumes than the older model. For larger mass fluxes, however, the new model predicts larger plumes than the older model. Because the Maat Mons summit elevation is already more than 9 km above the mean planetary radius, the reduced atmospheric pressure results in a plume with enough buoyancy to more than compensate for all of the model effects. These results continue to support the possibility that explosive eruptions on Venus may be capable of producing plumes that rise buoyantly to heights detected by the Pioneer Venus orbiter.

1. Introduction

The Pioneer Venus orbiter deployed to Venus in 1978 detected anomalously high concentrations of SO_2 at the top of the Venusian troposphere (~70 km above the mean planetary radius (ampr)). These initial measurements were followed by a steady decline in measured concentrations over the next 5 years. The observations by Pioneer Venus indicated that there is an episodic process currently supplying SO_2 to the upper Venusian troposphere. One possible mechanism for explaining such a phenomenon is explosive volcanism [*Esposito*, 1984; *Moore et al.*, 1992; *Robinson et al.*, 1995].

Whether or not volcanoes can erupt explosively on Venus has been the topic of debate for many years [*Head and Wilson*, 1986; *Wood and Francis*, 1987; *Thornhill*, 1993; *Robinson and Wood*, 1993; *Robinson et al.*, 1995]. The surface of Venus is subject to extremely high temperatures (~470°C) and pressures (up to 9.8 MPa). This means that the relative density difference between the erupted volcanic material and the ambient is much less than on Earth. The high pressure also means that it is much more difficult for volatiles to exsolve from the magma [*Wilson and Head*, 1983]. In addition, Magellan data have provided very little evidence that points to explosive volcanism [*Head et al.*, 1992]. Only a handful of fine-grained deposits associated with volcanoes have been identified [*Campbell*, 1994; *Campbell et al.*, 1998]. There is, however, some very compelling evidence in support of modern volcanism on Venus. First, a study by *Fegley and Treiman* [1992] investigated the chemical interactions that occur between the planet's surface and its atmosphere. The results of this study indicated that magma would have to be erupted at a rate of ~1 km^3/yr in order to supply SO_2 at a rate fast enough to keep up with scavenging by the surface/atmosphere chemical processes. Another independent study by *Solomon and Head* [1982] suggested that even higher rates of volcanism are necessary to

Paper number 1998JE000619.
0148-0227/99/1998JE000619$09.00

material consists of solid particulates and some magmatic volatile (either H_2O or CO_2). The mass flux of the solids and magmatic volatile within the control volume do not change with height. The ambient atmosphere on Venus below 100 km altitude is assumed to be composed of a variety of gaseous species based on spectroscopic observations and in situ measurements (see section 4 below). This ambient gas mixture, which includes some fraction of the species assumed to be the magmatic volatile, is entrained at each step along the rise height. It should be noted that the model formulation assumes that all of the plume components move confluently (no drag) and that no mass is lost as a result of sedimentation or rainout.

The final modification made here to the *Glaze et al.* [1997] model is the inclusion of a gas thrust, or jet, region at the base of the plume. In contrast to the convecting plumes that are driven primarily by buoyancy, plume rise in the jet region is dominated by momentum. *Wilson* [1976] was the first to model a volcanic plume as a jet, and *Woods* [1988] later combined the jet and buoyancy models. Following the Woods approach, the mass flux in the jet region can be defined as

$$\frac{d}{dz}(\rho_B u r^2) = \frac{ur}{8}(\rho_a \rho_B)^{1/2}. \quad (1)$$

When solving the system of equations, this definition for the mass conservation is used in place of (5) by *Glaze et al.* [1997] until the plume transitions to a convecting column. The point at which this transition takes place is discussed in more detail in the following section.

3. Comparison and Discussion

Two recent efforts to look at explosive volcanism on Venus have come from *Thornhill* [1993] and *Robinson et al.* [1995]. Both of these studies used the *Woods* [1988] model for volcanic plume rise. The model used in this study differs from *Woods* [1988] in three distinct ways, two involving the thermal energy conservation definition and one involving the transition between the momentum-driven and buoyancy-driven regions. These differences and their consequences will now be discussed in turn.

First, as noted by *Glaze and Baloga* [1996], the term in the *Woods* [1988] model that describes the cooling of the control volume due to entrainment of ambient air is inconsistent with the momentum conservation defined for the system. The second difference between the model presented here and the Woods model is also in the thermal energy conservation definition. The adiabatic cooling term in both the *Woods* [1988] and subsequent *Woods* [1993] models has been applied to the partial density of the gas phase (the density that the gas would have if it occupied the entire control volume, e.g., no particles) within the plume as opposed to the actual density. Of course, as the plume expands adiabatically and entrains additional gas, the relative volume occupied by the solids becomes very small.

Table 1. Notation

Variable	Definition
C_a	bulk atmosphere specific heat on Venus
f_i	mass fraction of constituent i
H	maximum plume height
n_0	gas mass fraction of magmatic volatile
r	plume radius
R_a	bulk atmosphere gas constant on Venus
R_u	universal gas constant (= 8.315 J K^{-1} mol^{-1})
u	bulk plume velocity
z	vertical distance
θ	bulk plume temperature
μ_i	molecular weight
ρ_a	bulk atmospheric density
ρ_B	bulk plume density

Table 2. Effect of Variations in the Thermal Energy Conservation Definition

	H, km			
r_0, m	*Glaze et al.* [1997]	Entrainment	Adiabatic	Both
20	9.3	9.8	9.2	9.8
50	15.1	16.0	15.1	16.0
100	20.0	20.8	20.0	20.8
150	22.8	23.7	22.8	23.7
200	25.0	26.0	25.0	26.0

Table 2 shows predicted plume heights for some typical boundary conditions on Earth and several variations on the thermal energy conservation term. The boundary conditions used in each of the model runs assumed $u_0 = 300$ m s^{-1}, $\theta_0 = 1000$ K, $n_0 = 0.03$ (where the volatile was water vapor), $z_0 = 0$ km, and r_0 is defined in the first column. For illustration purposes the plumes were erupted into a summertime tropical atmosphere, and no condensation was allowed. The maximum plume heights predicted by the *Glaze et al.* [1997] model are presented in the second column. The third column shows how the predicted plume heights are affected by changing only the entrainment term in the thermal energy equation to agree with *Woods'* [1988, 1993] expression. It can be seen that using the Woods entrainment term results in an overestimate of the maximum plume height by ~4–7% in these cases.

As stated above, the effect of using the partial density should be very small, and Table 2 verifies that this is indeed the case. The maximum plume heights presented in the fourth column for plumes where only the Woods adiabatic cooling term has been used are, in fact, indistinguishable from those predicted by the *Glaze et al.* [1997] model. The final column in Table 2 shows the cumulative results of using Woods' entire thermal energy expression. As expected, only the entrainment error can be detected by looking at the maximum predicted plume heights.

The third major difference between the Woods approach and the model used here is the definition of the transition between the momentum- and buoyancy-driven regions of the plume. While the expression for the conservation of mass flux given in (1) is identical to that used by *Woods* [1988], the transition between the jet and buoyancy regions is defined very differently here. The *Woods* [1988, 1993] models both assume that the plume becomes buoyant at the point where the bulk plume density drops below the ambient density. While, at first sight, this seems to be a logical assumption, it is not allowed by a self-consistent formulation of the governing equations. Under this assumption, the solutions for all of the variables (e.g., velocity, radius, and temperature) are discontinuous across the boundary, which is not acceptable in the physical world. The method used here for defining the jet/buoyancy boundary ensures that all of the variables have continuous solutions, and is defined in the following way. It is assumed that the plume is initially described by the jet model for entrainment. At each

on Venus is extremely dry [*Fegley and Treiman*, 1992] and that CO_2 is more likely the primary magmatic volatile species [*Head and Wilson*, 1986]. This choice is based on the conclusions of *Thornhill* [1993] and *Kieffer* [1995] that magmas with CO_2 as the primary volatile would not form convecting eruption columns. These conclusions are in agreement with results of the model presented here. As part of a complete discussion of boundary conditions for explosive plumes on Venus, *Thornhill* [1993] also concluded that plumes with initial temperatures of 1200 K would collapse and form pyroclastic flows unless the initial heat flux was greater than 2.05×10^{15} J s^{-1} (equivalent to an initial radius of 175 m for the boundary conditions listed above) and that plumes with initial temperatures below 1000 K would not convect at all on Venus.

Figure 3 compares maximum plume height results for both approaches. Because both approaches are based on the original *Morton et al.* [1956] buoyant plume formulation, the two models are in reasonable agreement, despite significant inconsistencies in the Woods approach. The results from the model used here continue to support the earlier findings of *Head and Wilson* [1986] that volatile contents in excess of 4 wt % are required to generate explosive volcanic plumes capable of rising to the top of the troposphere. All of these studies, however, contradict the contention of *Sugita and Matsui* [1992] that much lower mass and heat fluxes are necessary to drive a plume in excess of 45 km ampr.

The results shown in Figure 3 indicate that the Woods approach predicts plume heights that are consistently too high by about 5–8%. The extra altitude gained by those plumes is due to the combined use of the *Woods* [1988] ambiguous thermal energy definition and the criterion for the discontinuous transition. Figure 4 shows that the larger difference in plume

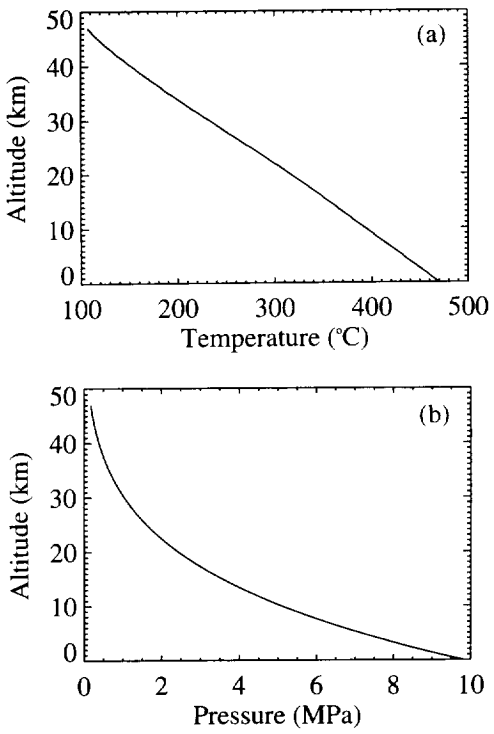

Figure 2. Globally averaged (a) temperature and (b) pressure profiles for the Venus atmosphere as taken from *Seiff* [1983].

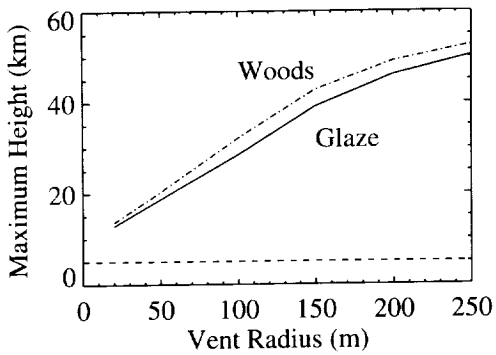

Figure 3. Comparison of the net effects of the Woods approach with the Glaze approach used here. The Venus boundary conditions used for both models were $u_0 = 270$ m s^{-1}, $\theta_0 = 1400$ K, $n_0 = 0.05$ (water vapor), and r_0 shown along the x axis. Note that the Woods approach has overestimated the maximum plume height due to both of the issues discussed in the text.

heights seen on Venus is primarily due to the use of the discontinuous solution across the boundary (note when comparing Figure 1 for Earth and Figure 4 for Venus that the vertical scales are not the same). It can be seen that, for the continuous solution, the altitude of the transition point is fairly insensitive to the initial radius (or mass flux). The discontinuous transition height, however, is systematically higher than the continuous solution and exhibits a significant dependence on initial radius. Use of the discontinuous solution implies that explosive jets of ash can extend up to 10 km above the vent on Venus. This means that for the discontinuous solution the plume is much higher when the buoyancy model begins describing the plume and that, consequently, the final plume is somewhat higher.

The fact that the Woods approach overestimates plume heights by 5–8% is an important result of this study in the sense that the difference is relatively small. The nonphysical discontinuous solutions and the lack of internal consistency in the Woods model make it difficult to assess the validity of the previous Venus applications and conclusions derived from the model. The analyses presented here clearly illustrate the relative magnitudes for each of the issues discussed above as well as the extent to which their relative magnitudes are magnified or minimized for conditions on Venus. Based on these analy-

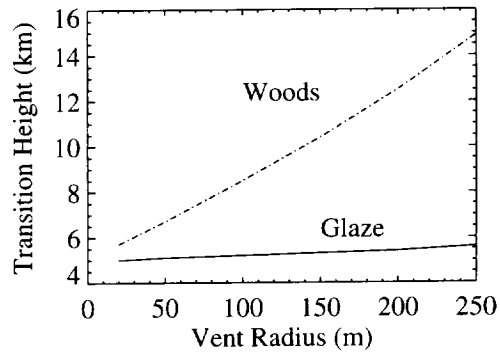

Figure 4. Comparison of the two methods for defining the jet/buoyancy transition for conditions on Venus. The boundary conditions used in both cases were $u_0 = 270$ m s^{-1}, $\theta_0 = 1400$ K, $n_0 = 0.05$ (water vapor), and r_0 shown along the x axis.

both studies are r_0 ranging from 20 to 300 m, θ_0 = 1400 K, u_0 = 270 m s^{-1}, z_0 = 9.17 km ampr, and n_0 = 0.05 water vapor. For small vent radii resulting in plumes that are barely buoyant, the Robinson et al. results overestimate the maximum plume height. This is the expected result based on the entrainment and transition issues described in section 3. However, for larger vent radii, the greater buoyancy of the plumes initiated at 9.17 km (as opposed to adding 9.17 to the height attained by a plume released at mpr) clearly outweighs the model effects, resulting in maximum plume heights even higher than those predicted by Robinson et al.

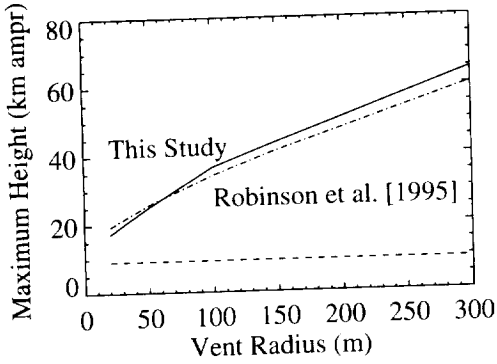

Figure 7. Comparison of maximum plume heights predicted by *Robinson et al.* [1995] with those predicted by the model presented here. Both models have been used to simulate an explosive eruption at Maat Mons with the boundary conditions u_0 = 270 m s^{-1}, θ_0 = 1400 K, n_0 = 0.05 (water vapor), z_0 = 9.17 km ampr, and r_0 shown along the x axis.

5. Conclusions

In this work, a new model based on the *Glaze et al.* [1997] approach has been used to reexamine the buoyant rise of explosive volcanic eruption plumes on Venus. This new model contains several improvements over the *Woods* [1988] model used in previous studies of explosive volcanism on Venus.

The model used here has corrected the formulation inconsistencies in the *Woods* [1988] model that result in a 4–7% overestimate of plume heights on Earth. This new model also redefines the criterion for the transition between the jet and buoyancy regions. The Woods discontinuous transition criterion results in an overestimate of the transition height as well as the maximum plume height and is magnified on Venus. The continuous solution appears to have very little dependence on initial vent size, whereas the discontinuous solution shows a very strong dependence on initial vent size. The continuous solution used here indicates that plumes on Venus become dominated by buoyancy effects almost immediately above the vent. The Woods approach, however, suggests that jets up to 10 km above the vent are possible for the boundary conditions considered. The combined effect of using the Woods approach for conditions on Venus is a 5–8% overestimate of the maximum plume height for vent radii ranging from 20 to 250 m.

The effects of latitude and elevation have also been explored. For large eruptions on Venus, plumes rising in the Northern Highlands would rise much higher than identical plumes erupted in the equatorial Lowlands. This is due to two effects. The first is that the upper atmosphere is more stable near the poles, resulting in a greater buoyancy effect for plumes that rise through that region. Second, vent elevation plays an important role in a plume's ability to become buoyant because of the sharp decrease in atmospheric pressure as a function of altitude.

To examine the net effect of all these influences, an eruption was simulated for conditions at Maat Mons and compared to results presented by *Robinson et al.* [1995]. These simulations indicate that for smaller initial mass fluxes (smaller vent radii), the plumes produced by the model presented here do not rise as high as the Robinson et al. plumes. Robinson et al. have overestimated these plume heights due to the cumulative effects of the inconsistencies in the *Woods* [1988] model. For larger mass fluxes (larger vent radii), however, Robinson et al. underestimate the maximum plume heights. This is due to the fact that Robinson et al. have erupted their plumes at mean planetary radius and then added the vent elevation on to the final plume height. However, because the initial elevation of the summit of Maat Mons is already more than 9 km ampr, the reduced atmospheric pressure results in a plume with enough buoyancy to more than compensate for all of the Woods effects.

These results continue to support the possibility that explosive eruptions on Venus may be capable of producing plumes that rise buoyantly to heights detected by the Pioneer Venus orbiter. The boundary conditions used to simulate such a plume are an initial vent radius of 300 m, an initial bulk plume temperature of 1400 K, an initial bulk plume velocity of 270 m s^{-1}, a vent elevation of 9.17 km ampr, and an initial magmatic water content of 5 wt %. It may be, however, that large buoyant plumes are not the only way to transport SO_2 and that other possibilities should be considered. The Venusian troposphere is well mixed, and it may be possible that circulation such as the Hadley Cell circulation on Earth could be capable of transporting volcanic material from smaller eruptions or from passively degassing vents through the troposphere [*Crisp et al.*, 1991]. The key to such transport would be the timescale of the circulation. It would be imperative that the transport be completed within the lifetime of the combined SO_2/H_2SO_4 cycle. On Earth, the complete conversion of volcanic SO_2 to H_2SO_4 can take several months (SO_2 was observed by satellite instruments more than 170 days after the Pinatubo eruption in 1991 [*Read et al.*, 1993]). Another possible mechanism for transporting volcanic SO_2 might be by co-ignimbrite eruption plumes that result from collapsing eruption columns. *Woods and Wohletz* [1991] have shown that co-ignimbrite plumes are capable of rising to great heights because most of the larger particles are sedimented out during pyroclastic flow, leaving only very fine particles and hot gas.

Acknowledgments. L. Glaze would like to thank the Geodynamics Branch at Goddard Space Flight Center for office space and continued support. Thanks also to S. Baloga for constructive comments throughout this work. This effort was funded by the NASA Venus Data Analysis and the Planetary Geology and Geophysics Programs (NASW-98012).

References

Briggs, G. A., *Plume Rise*, 80 pp., U.S. Atomic Energy Comm., Washington, D. C., 1969.

Campbell, B. A., Merging Magellan emissivity and SAR data for analysis of Venus surface dielectric properties, *Icarus*, *112*, 187–203, 1994.

Campbell, B. A., L. S. Glaze, and P. G. Rogers, Pyroclastic deposits on

APPENDIX B:

1999 Annual Report PRI Technical Report #V99-005

Proxemy Research is under contract to NASA to perform science research of volcanic plumes on Venus and Io. The following report constitutes delivery of ***Milestone Event #12*** under NASA contract NASW-98012.

TITLE: 1999 Annual Report: 'Volcanic Plumes on Venus and Io', **PRI Tech. Rep. # V99-005**.

AUTHOR: Lori S. Glaze

1. Introduction

Since funding for this project began in April 1998, we have successfully completed all of the milestones set out in contract NASW-98012. The project covered by this contract is comprised of two distinct tasks that were outlined in the original proposal entitled " Volcanic plumes on Venus and Io," dated May 29, 1997. The first objective was to produce a manuscript that presents results from previous work funded by the NASA Planetary Geology and Geophysics Venus Data Analysis program. A copy of the resulting manuscript "Transport of SO_2 by explosive volcanism on Venus" is submitted with this annual report and composes Appendix A. The second objective was to develop a model that constrains stochastic-ballistic effects of variable ejection velocities on areal concentrations of volcanic deposits on Io. A preliminary manuscript describing work conducted to date on this model is submitted with this report and is found in Appendix B.

2. Summary of Milestones 1, 2 and 3

Preparation of a one year Progress Report titled "Volcanic Plumes on Venus and Io" (NASW-98012) and project planning activities constituted the effort directed towards Milestone #1. Reviewing proposals for the NASA Planetary Geology and Geophysics program include activities for Milestones #2 and #3.

3. Summary of Milestone 4

Preparation of a manuscript entitled "Explosive Volcanism on Venus" comprises all hours contributed to Milestone #4. The manuscript was submitted to the Journal of Geophysical Research/Planets on August 31, 1998.

The rise of volcanic plumes on Venus was re-examined in this research using recent improvements in buoyant plume modeling. Two objectives were considered for this study. The first explored whether mechanisms governing plumes on Venus are capable of transporting SO_2 to the troposphere. The second objective studied the effects of ambient conditions due to variations in latitude and elevation.

Earlier models considering plume dynamics used non-physical discontinuous solutions for all modeling parameters and lacked internal consistency in governing equations. The entrainment term used in the thermal energy conservation equation is inconsistent with the momentum conservation defined for the system. In addition, an adiabatic cooling term applied to partial density of the gas phase (no particle entrainment) is used instead of actual density. The transition between the momentum driven (jet driven) and buoyancy driven regions also strongly contributes not only to transition boundary heights, but also to overall plume heights. The previous model assumes that the plume becomes buoyant at the point where the bulk plume density falls below the ambient air density. However, this assumption leads to discontinuous solutions for the model variables (radius, temperature, velocity) across the jet/buoyancy boundary.

The model used in this study is based on the Glaze et al. (1997) model. Changes include assumptions made for Venus' environment and the inclusion of a jet region at the base of the plume. This revised model uses continuous solutions for all modeling parameters and is internally consistent. While the net effect of correcting the adiabatic cooling term to accommodate actual plume density is negligible, the Glaze et al. (1997) approach to the thermal energy (consistent with the momentum conservation of the system) produces significantly different plume heights in comparison with the Woods approach. The jet/buoyancy boundary in the Glaze model is defined as the height where all of the variables converge for both models, thus ensuring a continuous progression across the boundary. Use of this continuous solution results in the boundary between jet and buoyancy regions being significantly lower than previously believed.

Using atmospheric temperature and pressure profiles on Venus, the effects of latitude and vent elevation on plume height were also studied. Results from the model used in this study show that plumes erupting at higher latitudes produced higher plumes than those erupted at lower latitudes. This behavior is the result of greater stability in the upper atmosphere at latitudes above 60°. Plumes erupting at higher elevation also rise higher than those that erupt at lower elevation because of the rapid decrease in surface pressure.

4. Summary of Milestones 5 and 6

Minimal activity was reported on this project for Milestones #5 and #6.

5. Summary of Milestones 7, 8 and 9

After submission of the Venus manuscript, work began on the second task of the Venus/Io project. The objective of this task is to determine the effects of a variety of energy distributions on areal concentrations of particles deposited by volcanic eruptions on Io. Event Milestones #7, #8 and #9 collectively addressed this objective. Energy distributions that were explored included uniform (fixed energy), simple correlated Gaussian, and Maxwell. Uniform and weighted angular distributions have also been considered for the fixed energy case.

The stochastic-ballistic model used in this study is an extension of that proposed by the Voyager Team (Cook et al., 1979) and Strom (1981) where particle trajectories are ballistic and are

governed by classical mechanics, except near the vent where stochastic behavior governs particle motion. The first case study performed considered a fixed energy eruption. Ejected particles were assigned a single velocity with ejection angles varying randomly between 0° and 90° from the vertical. The second case study considered a Gaussian distribution of energies with a prescribed mean velocity value and a relative standard deviation.

The next activity was to compare the dimensions of the annular deposit predicted by the model to those seen on Io. Galileo Solid State Imager (SSI) images were searched for a Prometheus-type of plume, which reaches 50-120 km in height, covers a region between 200-600 km radially away from its source, and is commonly associated with bright annular deposits. The near nadir view of Prometheus visible in Galileo SSI image #6578r on the G2 orbit was selected for study. The dimensions of the Prometheus annulus, including its width and radius, were collected. This completed Milestone #7.

Characterization of Prometheus' annular deposit was based on statistical analysis of several brightness profiles. The outer edge of the annulus was defined as the location of the break in slope between the average background DN value and the feature itself. The inner edge of the annulus was defined as the location where the background DN value within the profile was exceeded. The locations of the inner and outer edges of the annulus were collected for several brightness profiles that radiated from the summit of Prometheus. A summary of the statistical character of the annulus is summarized in the draft Io manuscript included as Appendix B to this report.

Preliminary conclusions drawn from this study suggest that variable energy eruptions can produce areal distributions of ejected particles that resemble the particle distributions observed in the Prometheus annulus. Brightness profile analysis and both fixed and variable velocity case studies completed Milestone #8.

Preliminary results from the stochastic and ballistic model were summarized in an abstract prepared for the 1999 Lunar and Planetary Science Conference. The draft manuscript in Appendix B contains the information included in the LPSC abstract. This completed Milestone Event #9.

6. Summary of Milestone Event 10

Further development of the stochastic-ballistic model was conducted. In addition, a poster presentation depicting preliminary research on stochastic-ballistic modeling was given at the 1999 Lunar and Planetary Science Conference.

7. Summary of Milestone Event 11

The stochastic-ballistic model was used to explore the effects of assuming independently varying velocity components. In this case, the two velocity components (v_x and v_z) have independent, uncorrelated Gaussian distributions. The resulting distribution of energies for this situation is Maxwellian. In addition, initial exploratory steps were taken to investigate the effects of ejection

angle on the resulting annulus. This completed Milestone Event #11.

8. Summary of Milestone Event 12

In the last month of the first year of this contract, the Venus manuscript described in Milestone #4 was accepted for publication, pending some revisions. These revisions were completed and the final manuscript was returned to JGR-Planets. The final version is included here as Appendix A. In addition, some time was spent conducting some proof of concept applications of the stochastic-ballistic model for inclusion in a full proposal to the NASA Planetary Geology and Geophysics Program.

9. Conclusions

This has been a very productive year for this project. Task 1 of the originally proposed work was completed and significant progress was made on Task 2. Under Task 1, a manuscript describing the transport of SO_2 on Venus via convecting volcanic plumes was prepared, submitted, revised and accepted for publication. This study showed that explosive volcanism is still a plausible mechanism for SO_2 transport to the top of Venus' troposphere. Under Task 2, a stochastic-ballistic model for volcanic eruptions on Io has been developed to address problems that surround mechanisms for creating annular deposits. Preliminary results for a variety of simple energy and angular distributions have been able to generate annuli with dimensions similar to those seen at Prometheus (Galileo image #6578r).

APPENDIX C:

Application of a Stochastic-ballistic emplacement model to volcanic eruptions on Io

Stochastic-ballistic eruption plumes on Io

Lori S. Glaze and Stephen M. Baloga

Proxemy Research, 20528 Farcroft Lane, Laytonsville, MD 20882

Accepted for publication in JGR/Planets
Revised: April 14, 2000

Abstract. Some active volcanoes on Io are associated with bright annular deposits. Here, we characterize the dimensions of the annulus observed at Prometheus. Assuming that relative brightness in images is directly related to areal particle concentration on the surface, we develop a model describing emplacement of particles whose motion is controlled by stochastic processes near the vent and ballistic transport beyond. Stochastic processes are expressed as probability distributions for the important transport variables. By varying the distribution parameters, high particle concentrations on the surface come and go. For isotropic ejection from the stochastic region with a fixed energy, subsequent ballistic transport to the surface produces singularities in the areal concentration at $r = 0$ and $r = r_{max}$. This areal concentration of particles features peaks corresponding to the singularities. Truncation of the ejection cone such that particles with a single energy are ejected isotropically between 0 and some maximum angle, θ_o removes the peak near the vent and increases the relative importance of the peak near r_{max}. Extrapolating the model with a Gaussian energy distribution introduces enough dispersion in the areal concentrations to produce broad annuli. Varying combinations of the truncation angle and RSD for the energy distribution changes the shape and magnitude of the surface deposit. A truncation angle of 75° and an RSD of .08 produces a symmetric annulus closest in shape and size to that observed at Prometheus. From examination of the energetics associated with thermalized particles, we find that many molecular compositions are admissible as annulus constituents at Prometheus.

1. Introduction

Volcanic plumes on Io and their deposits have been classified into two major classes. Prometheus-type eruptions are low, 50-120 km high, and have 200-600 km diameter surface deposits, and Pele-type eruptions have heights upwards of 300 km with deposits on the scale of a 1000-1500 km in diameter (McEwen and Soderblom, 1983). These plumes are thought to be driven by SO_2 and/or sulfur and be the source of the surrounding pyroclastic deposits (*e.g.* Smith *et al.* 1979; Strom *et al.*, 1981; Kieffer, 1982; Wilson and Head, 1983). Johnson *et al.* (1995) proposed a new class of plumes ('stealth' plumes) that are high entropy, pure gas eruptions of SO_2. However, McEwen *et al.* (1998) argue that Prometheus-type and 'stealth' plumes share many of the same characteristics.

Of these types of plumes, the Prometheus-type are commonly associated with bright annular deposits (McEwen and Soderblom, 1983; Figure 1), generally thought to be surface deposits of frozen SO_2 (Johnson *et al.*, 1979; Strom *et al.*, 1981; McEwen *et al.*, 1985). Recent results from Galileo also seem to indicate that Prometheus-type plumes are associated with high temperature (>1000 K) volcanism (McEwen *et al.*, 1998). Strom *et al.* (1981) state that the Prometheus plume, as viewed through the Voyager 1 clear filter, lies within the bright annulus. However, ultraviolet images of other plumes on Io imply that the clear filter significantly underestimates the plume size due to Rayleigh-like scattering by small particles in the UV range (Collins, 1981). In addition oblique Voyager images clearly indicate that ejected plume material reaches the bright annulus at Prometheus (Strom *et al.*, 1981).

The dimensions of the bright annuli are readily obtained from Voyager and Galileo data. Assuming that the annuli are deposits of ejected plume material, these dimensions provide an important constraint on the distribution of energies and velocities for pyroclast ejection and emplacement. Our assumption is that the brightness observed in Galileo and Voyager images of annuli and other bright volcanic deposits is proportional to the areal density of particles. Here we compare measured annulus dimensions with modeled areal surface density distributions to constrain admissible distributions of energy and ejection angles at the source. We also explore the nature of volcanism on Io (sulfur, basalt, or ultramafic) and molecular compositions of the ejecta (e.g., SO_2, elemental sulfur, or other sulfur compounds; McEwen *et al.*, 1985) that are consistent with observed plume dimensions.

Our approach is to further develop an idea presented in the early 1980's called the 'stochastic-ballistic model' (Baloga *et al.*, 1983). This model extended the pure ballistic and aerodynamic models developed by the Voyager team (Cook *et al.*, 1979) and Strom *et al.* (1981). As appropriate to the tenuous Io atmosphere, the stochastic-ballistic model assumes that the trajectories of plume particles are essentially ballistic and governed by classical particle mechanics, except for a limited region near the vent where stochastic effects are important. These stochastic effects include, collisions, thermalization, distributions of energy, randomization of velocity components, and irregularities in vent conditions. In studies of Pioneer 10 occultation data (Matson *et al.*, 1982), it was shown that the thermal velocity components of plume particles were comparable to the mean stream velocity of ejection. Other aspects of this theory were presented in connection with the bright auras surrounding many lava flows on Ra Patera (Baloga *et al.*, 1983).

We begin by describing, in detail, the annular feature observed in typical Galileo (or Voyager) images of Prometheus. We then present the basic stochastic-ballistic theory for a single energy eruption and completely isotropic ejection through the full range of ejection angles. Throughout the analysis we explore the admissible constraints on ejection parameters that result in the formation of high particle concentration annuli with dimensions and qualitative features similar to those observed at Prometheus. These constraints are based on random processes in the stochastic regime that produce an isotropic angular distribution within an ejection cone with various angles of truncation. We also consider the effects of a simple Gaussian energy distribution with various degrees of dispersion and truncation of the ejection cone. Finally, we speculate on using this theory of emplacement to constrain plume deposit compositions for different compositional styles of volcanism.

2. Prometheus Example of Annulus Dimensions

Figure 1 is an image of Prometheus in eruption captured by the Galileo Solid State Imager (SSI) on the G2 orbit (image 6578r). The image in Figure 1 was acquired with the red filter (.6 - .73 μm), and illustrates the typical bright annular deposit associated with Prometheus. For scale reference in the following theoretical study, we have used pixel units to characterize this annulus in terms of its mean dimensions, as well as

its variability. The pixel resolution at Prometheus is approximately 5 km.

Figure 2 shows four typical radial brightness profiles (as referenced back to Figure 1b). The bright annular feature is clearly visible in all the transects between about 20 and 40 pixels (~ 100 - 200 km) from the vent. The outer 'edge' of the feature (furthest from the origin) was found by visually locating the break in slope between the feature itself and the background brightness values. A sliding four point algorithm was used to help identify the break in slope. The algorithm simply subtracted the brightness at location (n-3) from that at location (n) for all pixels from n = 4 to the end of the transect. The last point with a negative slope in brightness was chosen as the outermost pixel of the annulus. The brightness value at that point was taken to be the cutoff value between background and annulus for that transect. The inner edge (closest to the origin) was defined as the location at which the background brightness value (for that transect) was exceeded. The inner and outer edges as defined by this approach are indicated by the solid square for each transect.

Table 1 indicates the distance (in pixel units) from the origin for both the inner and outer edges of the annulus for each transect. The transect numbers given in column 1 correspond to the numbers shown in Figures 1 and 2. As can be seen in Figure 1a, there is a break in the annulus east of the summit. For this reason, the group of three transects to the east (2, 14 and 16) are not included in Table 1 and have not been considered in the statistical estimate of annulus dimensions. In addition to showing the locations of the inner and outer edges of the annulus, the final column in Table 1 shows the distance from the origin for the brightest annulus pixel in the transect. As can be seen from Figure 2, this peak value may or may not correspond to the midpoint of the annulus.

Table 2 summarizes the statistics describing the dimensions of the Prometheus annulus. Based on the data in Table 1, the mean locations of the inner and outer annulus edges are 19 and 41, respectively. These annulus dimensions are very well constrained with standard errors on the order of 1 pixel. This implies that there is a 95% probability that the ± 2 pixel interval around the mean values will contain the 'true' location of the annulus edge. It should be noted that transects 4, 6, 10 and 11 show a slight difference in annular dimensions to the southeast of the volcano. From the data in Table 2, we conclude that the center of the annular feature is located approximately 30 pixels (~150 km) from the origin and that it has a width of approximately 22 pixels (~110 km). It is interesting to note that the mean location of peak brightness value is essentially the same as the midpoint of the annulus (within two standard errors).

Throughout the remainder of this paper, we will employ different applications of the stochastic ballistic model described in the following section in an effort to reproduce the areal concentration distribution of the Prometheus annulus described above.

3. Stochastic-Ballistic Model

The stochastic-ballistic model used throughout this paper divides a plume into two spatial regions. The stochastic region is considered to be a hemisphere near the vent with a radius that is small compared to the overall dimensions of the plume (Figure 3). Within this region, the random effects associated with collisions of particles, thermalization, irregularities in vent condition, and perhaps phase changes, dominate the ejection. In general, we will assume that the important transport variables (e.g., energy, momentum, ejection angles) have probability distributions. Once particles leave the stochastic region, the randomizing influences on particle motions cease and the subsequent trajectories are purely ballistic. In effect, the probability distributions are quenched when the plume particles exit the stochastic region. The distributions of transport variables for the stochastic region thus serve as initial conditions for ballistic emplacement.

In this work, we are concerned with the areal concentrations of plume particles on the surface of Io that result from different distributions of transport variables in the stochastic region. All of the mathematical notation for the following discussion is defined in Table 3. We will assume that the plume is axisymmetric and use a cylindrical coordinate system to describe particle trajectories.

Basic Ejection Angle Considerations

We first consider the simplest case of ejection of N particles with a single energy to illustrate the stochastic-ballistic approach. Figure 3 shows the hemisphere that defines the boundary of the stochastic region. The probability that a particle is ejected into the thin, horizontal ribbon defined by $d\theta$ is

$$P(\theta) = \frac{dN}{N} = C\Theta(\theta)\sin\theta d\theta \qquad (1)$$

where C is a constant chosen for normalization and $\Theta(\theta)$ is the angular probability distribution measured from the vertical axis. Note from (1) that the probability of a particle being ejected at an angle, θ, is the same as the fraction of total particles ejected at that angle. If we limit the ejection cone to a maximum angle of θ_o , the normalization constant can be determined and (1) becomes

$$P(\theta)=\frac{dN}{N}=\frac{\Theta(\theta)\sin\theta d\theta}{\int_0^{\theta_o}\Theta(\theta)\sin\theta d\theta} \qquad (2)$$

For uniform, or near-uniform, gas expansion at the vent, particles should be ejected isotropically (Collins, 1981). An isotropic distribution requires that the number of particles per unit area be the same over the entire hemispherical limit of the stochastic region. Under this constraint, Θ = 1 and the distribution of ejection angles is

$$P(\theta)=\frac{dN}{N}=\frac{\sin\theta d\theta}{1-\cos\theta_o} \qquad (3)$$

which is normalized in the sense that

$$\int_0^{\theta_o}P(\theta)d\theta=1 \qquad (4)$$

To convert the isotropic distribution in (3) to an areal distribution on the ground, we need to rewrite all the θ terms as functions of r:

$$P(\theta(r))=\frac{dN(r)}{N}=\frac{\sin\theta(r)}{1-\cos\theta_o}\left|\frac{d\theta}{dr}\right|dr \qquad (5)$$

The absolute value on the right hand side of (5) comes about because we do not care whether dr is directed away from or toward the origin.

Fixed Energy Relationship Between θ and r

Our objective is to relate a distribution of particle energies in the stochastic region to an areal concentration of particles on the surface. In the simplest case, we assume a fixed energy for all particles. When combined with the concept of isotropic ejection, the areal concentration can be obtained analytically even when the ejection cone is limited to some arbitrary value.

If we define the ejection velocity for the fixed energy eruption to be v_o, and the radial and vertical velocity components, respectively as v_r and v_z, we know that,

$$v_o^2 = v_r^2 + v_z^2 = constant \qquad (6)$$

and

$$r=\frac{2v_rv_z}{g}=\frac{2v_o^2\cos\theta\sin\theta}{g} \qquad (7)$$

where (7) is the standard range equation for a ballistic projectile found in most physics texts (e.g., Halliday and Resnick, 1977). We note immediately that (7) can be rewritten as

$$\frac{gr}{2v_o^2}=\sin\theta\sqrt{1-\sin^2\theta} \qquad (8)$$

Squaring both sides of (8) and rearranging results in a quadratic expression in $\sin^2\theta$. Solving the quadratic gives

$$\sin^2\theta=\frac{1\pm\xi}{2} \qquad (9)$$

where

$$\xi=\sqrt{1-(r/r_{max})^2} \qquad (10)$$

and r_{max} is the maximum deposition distance found from (6) and (7) when $v_r = v_z$:

$$r_{max} = \frac{v_o^2}{g} \quad (11)$$

We can see from (9) that for $0 \le r \le r_{max}$, there are two trajectories that emplace particles at a distance r from the vent. This translates into ejection angles originating in the upper ($\theta < 45°$) and lower ($\theta > 45°$) portions of the plume for the '-' and '+' solutions, respectively.

Relation between dθ and dr

Now we ask, "If particles are ejected into some dθ, what is the corresponding dr on the surface?". We differentiate the second part of (7) to obtain

$$\frac{g\,dr}{2v_o^2} = \frac{dr}{2r_{max}} \left(\cos^2\theta - \sin^2\theta\right) d\theta = \left(1 - 2\sin^2\theta\right) d\theta \quad (12)$$

Hence,

$$\left|\frac{d\theta}{dr}\right| = \frac{1}{2r_{max}\left(1-\sin^2\theta\right)} = \frac{1}{2\xi r_{max}} \quad (13)$$

With the absolute magnitude on the left hand side of (13), we ignore a minus sign in one part of the right hand side that indicates r decreases when θ continues to increase beyond 45 degrees.

Conversion of angular ejection distribution to areal distribution

Substituting (9) and (13) into (5) we get

$$P(\theta(r))\frac{dN}{N} = \frac{1}{1-\cos\theta_o}\sqrt{\frac{1\pm\xi}{2}}\frac{dr}{2\xi r_{max}} \quad (14)$$

noting that the appropriate sign must be taken for a given θ or range of θs. Equation (14) gives the fraction of the total particles ejected that land in the annulus of width dr at a distance r from the vent.

Our assumption is that the brightness observed in Galileo and Voyager images of annuli and other bright volcanic deposits is proportional to the areal density of particles, ρ(r). To interpret (14) as an areal density at r we must consider the area of the annulus:

$$P(\theta(r)) = \frac{dN(r)}{N} = \rho(r)2\pi r dr \quad (15)$$

From (14) and (15) we are able to solve for the areal density as a function of radial distance. Because of the dependence of (14) upon the maximum ejection angle, the explicit solution for areal density is actually two sets of equations. If we note that particles ejected at θ_o will be deposited at a corresponding radial distance, r_o (= 2 $r_{max}\sin\theta_o\cos\theta_o$), then for $\theta_o \le 45°$,

$$\rho(r) = \frac{1}{1-\cos\theta_o}\frac{1}{4\pi r}\frac{1}{\xi r_{max}}\sqrt{\frac{1-\xi}{2}} \quad (16a)$$

for $0 \le r \le r_o$, and

$$\rho(r) = 0 \quad (16b)$$

for $r_o \le r \le r_{max}$. Similarly, for $\theta_o > 45°$, the areal density is given by

$$\rho(r) = \frac{1}{1-\cos\theta_o}\frac{1}{4\pi r}\frac{1}{\xi r_{max}}\sqrt{\frac{1-\xi}{2}} \quad (16c)$$

for $0 \le r \le r_o$, and

$$\rho(r) = \frac{1}{1-\cos\theta_o}\frac{1}{4\pi r}\frac{1}{\xi r_{max}}\left(\sqrt{\frac{1-\xi}{2}},\sqrt{\frac{1-\xi}{2}}\right) \quad (16d)$$

for $r_o \le r \le r_{max}$.

It is important to note that (16) has a fundamental singularity at $r = r_{max}$ resulting solely from the ballistic trajectories and a fixed energy. Ultimately, this is what counters the 1/r decay one might expect and produces the observed bright annuli on the surface of Io.

4. Example Applications

Here we present results of the basic model for a single energy eruption and then we explore possible

approaches to generating annular deposits with dimensions similar to those observed at Prometheus. In the first case, we simply truncate the ejection cone such that particles with a single energy are ejected isotropically between 0 and various maximum angles from the vertical. Next, we undertake a simple extrapolation of the basic model to allow for a normal distribution of eruption energies. In this instance, the energies are prescribed according to a Gaussian probability distribution, and the individual velocity components are correlated, i.e., if one velocity component is chosen at random, the other is determined exactly due to the energy constraint. We then explore the effects of ejection cone truncation and different levels of energy dispersion around the mean values on the shape of the areal concentration distribution. In all of the examples shown below, the areal concentrations at r are integrated over the length of a pixel.

Single Energy with Isotropic Ejection between 0 and 90°

Figure 4 shows the areal concentration of particles found on the surface by applying (16) when r_{max} = 39 (in pixel units) and $\theta_o = 90°$. The particles contributing to the high concentration peak near the vent all originate in the lower plume with ejection angles near 90°. This peak is due, in part, to the isotropic constraint on the distribution of ejection angles. The isotropic requirement results in the largest fraction of particles being ejected near 90°. At such high ejection angles, particles fall rapidly to the surface very near to the vent. The sheer number of particles, along with the relatively small surface area for small r, combine to produce the peak near the vent.

While this simple, single energy example illustrates the basic concepts of the stochastic-ballistic model, the resulting distribution of particles on the ground does not have the broad peak that is characteristic of the Io annuli. There is, however, a relative maximum near r_{max}, indicating that introduction of some variability into the velocity or ejection angles might result in a broader maximum.

In the remainder of this section, we explore three possible approaches that all result in annular deposits of high particle concentrations. By varying the parameters of these distributions, we can adjust the location and width of the annulus.

Single Energy with Truncated Isotropic Ejection between 0 and θ_o

To examine the sensitivity of the areal surface distribution to the maximum ejection angle, we simply truncate the ejection cone at some angle, θ_o. In general, we will assume that the ejection cone is cutoff at some angle less than 90° and that the distribution of ejection angles is isotropic for $0 \le \theta \le \theta_o$, with relatively few particles ejected beyond θ_o.

As discussed above, particles ejected at large angles are the source for the peak in particle concentrations observed near the vent in the single energy case. Figure 5 illustrates the effect of truncating the ejection cone at several choices for θ_o: 75°, 45°, and 20°. In all of these cases, we still consider a single energy and isotropic angular ejection. It should be noted that the value of r_{max} for $\theta_o = 20°$ has been chosen in order to produce a deposit of similar dimensions to the other two cases. Figure 5a shows that the peak near the vent is completely eliminated by truncating the ejection cone at 75°. Figures 5b and 5c illustrate how the concentration of particles on the ground can be changed simply by changing the maximum ejection angle. For θ_o = 45° the distribution increases exponentially out to r_{max}. For a narrow ejection cone with $\theta_o = 20°$, the concentration of particles on the surface is nearly constant from the vent out to r_{max}.

Figure 5 clearly illustrates just how sensitive the areal distribution is to the maximum ejection angle. Another indication of this sensitivity is evidenced by the discontinuity in the concentration 20 pixels from the vent for the 75° ejection cone (i.e., the lower plume does not contribute to the deposit between 0 and 20 pixels). If, however, we allow for a small tail in the angular distribution beyond the cutoff angle, the sufrace concentration should have a smoother appearance. The Fermi function is often used to describe boundary layers such as this and will be explored in future work.

Gaussian Energy Distribution (Correlated Velocity Components)

The fixed energy solutions shown in Figures 4 and 5 all indicate a maximum in areal concentration at r = r_{max}. In order to broaden the maximum such that it begins to resemble the annulus at Prometheus described above, we must find some way to diffuse the solution at this location. One way to accomplish this is to assume that instead of a fixed energy eruption, particle velocities come from a distribution that has a mean value, $\bar{v}$, and a standard deviation, σ.

The most natural choice for a velocity

distribution is the Gaussian or normal probability distribution. There is abundant evidence from numerous physics disciplines that when many different random variables combine, the resulting distribution tends to be Gaussian, regardless of the distribution of the individual random variables. This is often referred to as the 'central limit theorem' from probability theory (e.g., Larson, 1974) and is the basis for our use of the normal distribution.

Independent of the chosen probability distribution, and recalling from (11) that r_{max} can be written as a function of v_o, we re-write (11) for the case of distributed velocities as

$$r_{max}(v_f) = \frac{v_f^2}{g} \qquad (17)$$

where

$$v_f = \bar{v} + f\sigma \qquad (18)$$

and f is the fraction of the standard deviation derived from the probability distribution (= 0, ± 0.2, ± 0.4, etc.). Recalling that the Relative Standard Deviation (RSD) is simply the standard deviation divided by the mean value, we can re-write (18) as

$$v_f = \bar{v}(1 + f \cdot RSD) \qquad (19)$$

Substituting (19) back into (17),

$$r_{max}(v_f) = r_{max}(\bar{v})[1 + f \cdot RSD]^2 \qquad (20)$$

By choosing $r_{max}(\bar{v})$ such that the resulting annulus is centered 30 pixels from the vent, and varying the RSD, we can calculate $\rho(r)$ for each velocity, v_f.

To determine the fraction of particles ejected at a particular velocity, we now assume that the velocities are normally distributed (Gaussian). Under this assumption, we note that the cumulative probability between - .1σ and .1σ, inclusive, is equal to 0.0796. Thus, we would expect 7.96% of the particles to have velocities $(\bar{v} - .1\sigma) \le v \le (\bar{v} + .1\sigma)$, or $v \approx \bar{v}$. Similarly, we have found the fraction of particles having velocities in each .2σ interval from -4.1σ to 4.1σ.

The individual $\rho(r)$'s, determined by substituting the resulting r_{max}'s from (20) into (16), are then multiplied by the fraction of the total number of particles that are erupted with a velocity v_f. This fraction is determined from the normal probability distribution as described above (e.g., $\rho(r)$ is multiplied by 0.0796 for $v_f \approx \bar{v}$). Summation at each location, r, for contributions from all v_f's results in the total areal concentration, ρ, as a function of the distance, r, from the source.

Figure 6 shows the resulting areal concentration of particles as a function of radial distance from the source for four choices of the maximum ejection angle. In all cases, we have chosen an r_{max} such that the peak in areal concentration is centered around 30 pixels from the source and we have examined a range of RSDs in order to explore the sensitivity of the annular dimensions to small changes in RSD.

For isotropic ejection between 0 and 90°, the ground concentration of particles is still dominated by the peak near the vent due to the relatively large number of particles ejected at 90° (as a result of the isotropic constraint) that don't go any distance. As expected, a small RSD of 1% results in a very narrow annulus located near r_{max}. However, it is impossible to generate an annulus for θ_o = 90°. As the RSD is increased, the location of the peak moves inward (toward the source) slightly, and becomes broader. This small 'blip' is far too narrow to correspond to anything like what is observed at Prometheus and for RSD > 8%, the ground concentrations slowly decay to zero.

Truncation of the ejection cone at 75° can generate a variety of annular shapes simply by adjusting the RSD. All of the annuli shown in Figure 6b have dimensions comparable to the Prometheus annulus discussed above. By varying the RSD, we can modify the shape of the peak from a spike at the distal end (RSD = 1%) to a smooth, almost symmetric peak (RSD = 8%). For ejection between 0 and 45° (Figure 6c) all choices of RSD produce broad, asymmetric peaks of dimensions similar to those observed at Prometheus.

For completeness, we have shown what happens with a normally distributed energy when the ejection cone is truncated at 20°. The results shown in Figure 6d for two choices of RSD do not vary greatly from the single energy case shown in figure 5c.

In summary, we can easily make annuli of varying shapes and relative intensities by simultaneously adjusting the maximum angle of the ejection cone and the

RSD of a normally distributed energy.

5. Discussion

Prometheus is one of the most persistent volcanic centers on Io. It was observed to have an active plume during both Voyager encounters (Strom *et al.*, 1981) and has been consistently active during the current Galileo mission (McEwen *et al.*, 1997; 1998). During the intervening years between Voyager and Galileo, a dark lava flow was emplaced on the surface, indicating that Prometheus has of a range of eruptive styles. The lava flow is about 70 km long with the 1979 explosive vent at its eastern extent, and the new plume source at its western end (McEwen *et al.*, 1998). In 1979, the active plume was reported to be approximately 272 km in diameter with a height of 77 km, as measured in the clear filter (Strom *et al.*, 1981). Based on clear and UV observations of Loki (Strom *et al.*, 1981), plumes may have diameters up to two times larger in the UV than in the clear. Thus, the diameter of the Prometheus plume could exceed 500 km, extending to the outer edge of the bright annulus (reported as 330 km). McEwen *et al.*, (1998) indicate that Galileo observes a plume that has about the same dimensions and brightness as seen by Voyager.

Most people agree that either SO_2 or S_2 is the primary volatile driving explosive volcanism on Io. However, there is still debate as to what plume constituent is observed in satellite imagery. Kieffer (1982) suggested that the plumes may contain a significant population of SO_2 'snowflakes'. Based on observations at Loki, Collins (1981) concluded that the plume was comprised of two particle populations with radii of 0.001 - 0.01 μm and > 1 μ, respectively. Collins also states that the symmetric distribution of the smaller particles is consistent with isotropic ejection of the Kieffer 'snowflakes'. Recent work by Spencer *et al.* (1997) using observations by the Hubble Space Telescope indicate that there are two scenarios for explaining the wavelength dependence of the optical depth observed at Pele. The first is a fine 'dust' with a minimum mass of 1.2×10^9 g and a maximum particle size of 0.08 μm. The second scenario assumes SO_2 gas with a column density of 3.7×10^{17} cm^{-2} and a total mass of 1.1×10^{11} g.

With further study of the underlying physics of the stochastic regime, we believe the stochastic-ballistic approach could engender compositional constraints from the dimensions of the annular plume deposits. If the ejection of plume particles is envisioned as a continuously repeated release of particles from classical kinetic theory condition, then the thermal energy is available as kinetic energy to transport the particles through the ballistic region. Thus, as a crude estimate of the energy available, we can set

$$\frac{1}{2}mv_o^2 = \frac{3}{2}kT = \frac{1}{2}mgr_{max} \qquad (21)$$

Table 4 shows the ranges of particles, by atomic weight, in the first column and plausible plume temperatures in the first row. The atomic weights were chosen to include compositions ranging from S_2 or SO_2 to S_8. Temperatures in columns 2, 3, and 4 include those that might be associated with sulphur, basalt, and ultramafic volcanism, respectively. The cells corresponding to a unique combination of temperature and atomic weight indicate the predicted maximum plume radius (r_{max}) using (23). Based on observations by Strom *et al.* (1981), acceptable r_{max}'s should range between approximately ~135 and 250 km. These radii are consistent with the ~200 km maximum annulus extenet reported in Table 2.

From Table 4 we see that those (bold italic) species in the lower left quadrant are too small and those in the top right corner are too large. These combinations of volatile composition and temperature are precluded at Prometheus by the stochastic ballistic theory on the basis of thermal energy considerations. Based on NIMS observations, Prometheus appears to have a thermal component in excess of 1000 K (McEwen *et al.*, 1998), indicating that the columns with T = 1200 and 1800 K are the most probable. It is our belief that a more detailed consideration of the ejection physics would extend the admissible compositions to higher atomic weight particles. Nevertheless, the ranges shown suggest that the theory is sufficiently plausible in this regard to warrant further investigation.

6. Conclusions

In this work, we have explored three possible approaches to generating high particle concentration surface annuli for stochastic-ballistic plumes on Io. These three approaches were isotropic, fixed energy ejection; simple truncation of the ejection cone for a single energy isotropic eruption; and a Gaussian distribution of particle speeds for a range of ejection

cones. The areal concentrations predicted in these cases span a broad range of possible surface deposits, some of which feature annuli, while others do not.

The areal density predicted by the stochastic ballistic theory has a fundamental singularity at r_{max} that results solely from the ballistic trajectories and a fixed energy. Ultimately, this is what counters the 1/r decay one might expect and produces the observed bright annuli on the surface of Io. While there is more work to be done in order to constrain eruption conditions on Io, this work clearly indicates that the stochastic-ballistic model can easily predict a range of areal surface distributions assuming a variety of angular and energy distributions. Plausible ranges of distributions result not only in annuli, but also exponential decay as well as constant concentrations.

One important conclusion of this work is the influence of the ejection cone on areal concentrations. Due to the geometrical considerations of ejection into a hemisphere, the angular distribution of particles from the stochastic region emerges as a critical variable for the existence of annuli. We have shown that for isotropic ejection through a cone extending out to 90°, it is not possible to generate an annulus. However, by varying the maximum ejection angle, we can easily manipulate the amplitude and location of the high concentration, bright deposit.

Here, we have concentrated on the annulus at Prometheus observed by Galileo SSI. This annulus is very regular in its dimensions. We are able to tightly constrain the width of the annulus as 22 pixels (~110 km) and the location as 30 pixels (~150 km) from the source. Based on the 16 transects used to determine these dimensions, the uncertainties are all ± 2 pixels.

The single energy, isotropic angular distribution produces ground concentrations of particles with a relative maximum at a distance r_{max} from the source. This relative maximum is sharply cut off beyond r_{max} and does not resemble the dimensions of the Prometheus annulus.

The simple and logical first choice of a normal energy distribution does result in an annular feature with a relatively high concentration of particles. The location of this annulus can be adjusted by varying the choice for r_{max} corresponding to the mean energy, and the width of the annulus is controlled by the RSD of the energy distribution. For $\theta_o = 90°$, a choice of a small RSD (1%) results in a relatively high concentration, but very narrow (only 2 - 3 pixels) annulus. By increasing the RSD, we can broaden the peak slightly (to ~ 5 pixels), but the concentration of particles decreases to the point that an annulus is no longer visible by RSD = 8%. Thus, for annuli with dimensions similar to those observed at Prometheus, the normal energy distribution with isotropic angular distribution to 90° can also be precluded.

Truncation of the ejection angle combined with normally distributed energies results in annuli with dimensions comparable to that observed at Prometheus. Variations in θ_o and RSD can modify the intensity and shape of the annulus. Of the cases explored here, the Gaussian energy distribution with a maximum ejection angle of 75° is most similar to the dimensions observed at Prometheus. The most symmetric of these areal deposits occurs when r_{max} $(\bar{v}) \approx 38$ and for RSD = 8%. However, several of the other Gaussian parameters are also similar to individual Prometheus transects, and cannot be precluded.

In the future, it will be interesting to explore the possibility of anisotropic angular distributions, particularly in light of the sensitivity to angular dependence that we have demonstrated. To help further constrain the nature of the stochastic processes near the vent, the obvious next step will be to compare the geometry of plumes observed on Io's limb to the ballistic trajectories predicted by the subset of velocity and angular distributions that are consistent with the areal constraints. In this way, we hope to preclude some of the distributions that could not possibly produce plumes of the dimensions observed. We recognize that a variety of optical effects may influence the way in which we visualize remote sensing imagery. We will consider the photometric properties of the most probable plume constituents (SO_2, H_2S, etc.) in future work.

Acknowledgements

The authors would like to thank Bruce Hapke and Bob Nelson for constructive reviews of this manuscript and the Geodynamics Branch at Goddard Space Flight Center for office space and continued support. Thanks also to Jeff Plescia for assistance with Galileo imagery. SB would like to thank Dennis Matson for numerous insightful conversations that ultimately inspired this work. This effort was funded by the NASA Planetary Geology and Geophysics Program (NASW-98012 and NAG5-7251).

References

Baloga, S.M., D.L. Matson, and D.C. Pieri (1983) Auras and Io regolith outgassing by sulphur flows. *Lunar*

and Planetary Science Conference XIV.

Cook, A.F., E.M. Shoemaker and B.A. Smith (1979) Dynamics of volcanic plumes on Io. *Nature* **280**:743-746.

Collins, S.A. (1981) Spatial color variations in the volcanic plume at Loki, on Io. *J. Geophys. Res.* **86**:8621-8626.

Halliday, D. and R. Resnick (1977) **Physics, 3rd Edition**. John Wiley and Sons, New York.

Johnson, T.V., A.F. Cook II, C. Sagan and L.A. Soderblom (1979) Volcanic resurfacing rates and implications for volatiles on Io. *Nature* **280**:746-750.

Johnson, T.V., D.L. Matson, D.L. Blaney, G.J. Veeder, and A.G. Davies (1995) Stealth Plumes on Io, *Geophys. Res. Letters*, **22**, 3293.

Kieffer, S.W. (1982) Ionian Volcanism, in *Satellites of Jupiter*, D. Morrison, ed., Univ. of Ariz. Press, 647-723.

Larson, H.J. (1974) *Introduction to probability theory and statistical inference, 2nd ed.* John Wiley and Sons.

Matson, D. L., T. V. Johnson and S. M. Baloga (1982) Pioneer 10 Io Occultation Revisited: Path Through Volcanic Plume Gas? *EOS* **63**:1022.

McEwen, A.S. and L.A. Soderblom (1983) Two classes of volcanic plume on Io. *Icarus* **55**:191-217.

McEwen, A.S., D.L. Matson, T.V. Johnson and L.A. Soderblom (1985) Volcanic hot spots on Io: Correlation with low-albedo calderas. *J Geophys Res* **90**:12,345-12,379.

McEwen, A.S., L. Keszthely, D. Simonelli, M. Carr, R. Greeley, and the Galileo SSI team (1997) 17 years of surface changes on Io: Galileo SSI results. *Lunar and Planetary Science Conference XXVIII.*

McEwen, A.S., L. Keszthelyi, P. Geissler, D.P. Simonelli, M.H. Carr, T.V. Johnson, K.P. Klaasen, H.H. Breneman, T.J. Jones, J.M. Kaufman, K.P. Magee, D.A. Senske, M.J.S. Belton and G. Schubert (1998) Active volcanism on Io as seen by Galileo SSI. *Icarus* **135**:181-219.

Smith, B.A. and the Voyager Imaging Team (1979) The Jupiter System through the eyes of Voyager 1. *Science* **204**:951-972.

Spencer, J.R., P.Sartoretti, G.E. Ballester, A.S. McEwen, J.T. Clarke and M.A. McGrath (1997) The Pele plume (Io): Observations with the Hubble Space Telescope. *Geophys. Res. Letts.* **24**:2471-2474.

Strom, R.G., N.M. Schneider, R.J. Terrile, A.F. Cook and C. Hansen (1981) Volcanic eruptions on Io. *J. Geophys. Res.* **86**:8593-8620.

Wilson, L. and J.W. Head (1983) A comparison of volcanic eruption processes on Earth, Moon, Mars, Io and Venus. *Nature* **302**:663-669.

Figure Captions

Figure 1: Image of Prometheus showing the (a) bright annular deposit surrounding the volcano and (b) the transects (identified in Table 1) used to examine radial changes in brightness. The image was acquired by the red filter of the Galileo SSI on the G2 orbit (image 6578r) and is approximately 1000 km across.

Figure 2: Four typical radial transects showing variations in brightness as a function of distance from the summit. The 'boxes' correspond to the inner (closest to the vent) and outer edges of the annulus as defined by the algorithm described in the text.

Figure 3: Schematic diagram of a stochastic-ballistic plume showing the hemispherical stochastic region near the vent and the ballistic trajectory of a particle ejected at an angle θ. Note that the figure is not to scale. In reality, the stochastic region is very small compared to the scale of deposition (having a radius < 1 pixel unit).

Figure 4: Model results for a single energy eruption with r_{max} = 39 pixels and $\theta_o = 90°$.

Figure 5: Areal concentrations for a single energy eruption with θ_o = (a) 75°, (b) 45°, and (c) 20°. Values for r_{max} are 39, 39, and 59, respectively. Note that the large peak near the vent is nonexistent, even for $\theta_o = 75°$. See text for discussion of the abrupt cutoff at 20 pixels.

Figure 6: Areal concentrations for an eruption with normally distributed energies and θ_o = (a) 90°, (b) 75°, (c) 45°, and (d) 20°. In each case a variety of RSD's from 1 - 8% are shown. In order to achieve an annulus centered at a distance ~30 pixels from the vent, values for r_{max} ($\bar{v}$) are chosen as 30, 38, 35, and 60, respectively.

Table 1. Annulus dimensions for Prometheus image

Transect #	Distance From Origin (pixels)		
	Inner Edge	Outer Edge	Location of Peak DN
1	11	33	26
3	18	38	27
4	26	42	31
5	17	40	27
6	23	37	28
7	17	40	24
8	21	38	27
9	17	47	31
10	19	43	29
11	21	44	31
12	19	44	26
13	18	41	26
15	15	43	24

Table 2. Annulus statistics

Statistic	Distance From Origin (pixels)		
	Inner Edge	Outer Edge	Location of Peak DN
Mean Value	19	41	27
Standard Deviation	4	4	3
Standard Error	1	1	1

Table 3. Notation

Parameter	Definition
C	Normalization constant
f	Fraction of standard deviation
g	Acceleration due to gravity
k	Boltzmann constant
N	Number of particles ejected
P	Probability distribution
RSD	Relative Standard Deviation
r	Radial distance
r_o	Radial distance corresponding to θ_o
r_{max}	Maximum deposition distance
T	Temperature
$\bar{v}$	Mean velocity of distribution
v_o	Fixed ejection velocity
v_f	Velocity from distribution at fσ
v_r	Radial velocity component
v_z	Vertical velocity component
Θ	Angular distribution
θ	Ejection angle
θ_o	Ejection cone truncation angle
ρ	Areal concentration of particles
σ	Standard deviation of velocity distribution

Table 4: Maximum annulus radius from conversion of thermal energy to kinetic energy

Atomic Weight	T=600K	T=1200K	T=1800K
32	260	***519***	***779***
64	230	260	***389***
128	***65***	130	195
256	***32***	***65***	***97***

APPENDIX B

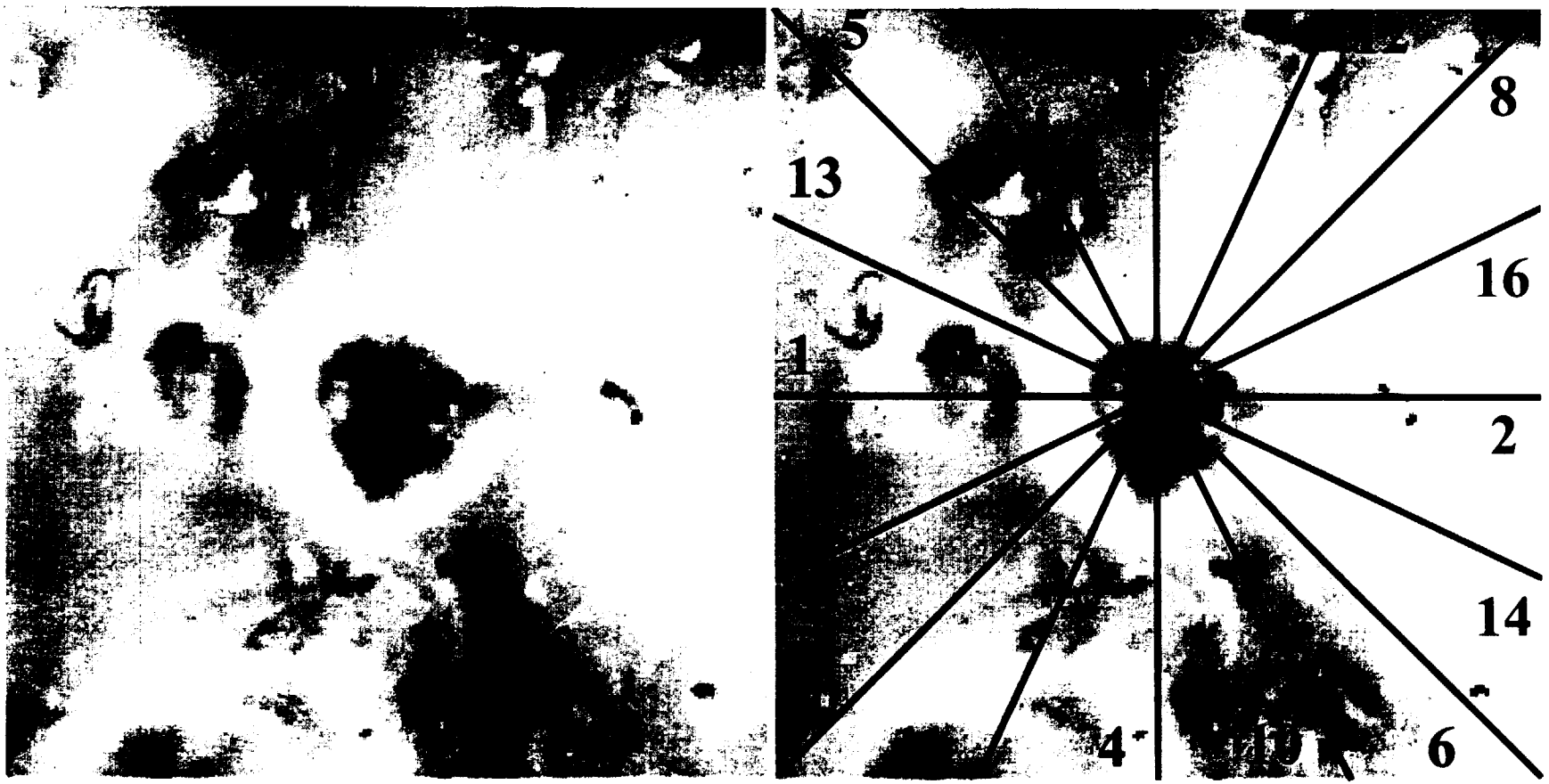

Glaze and Baloga

Figure 1

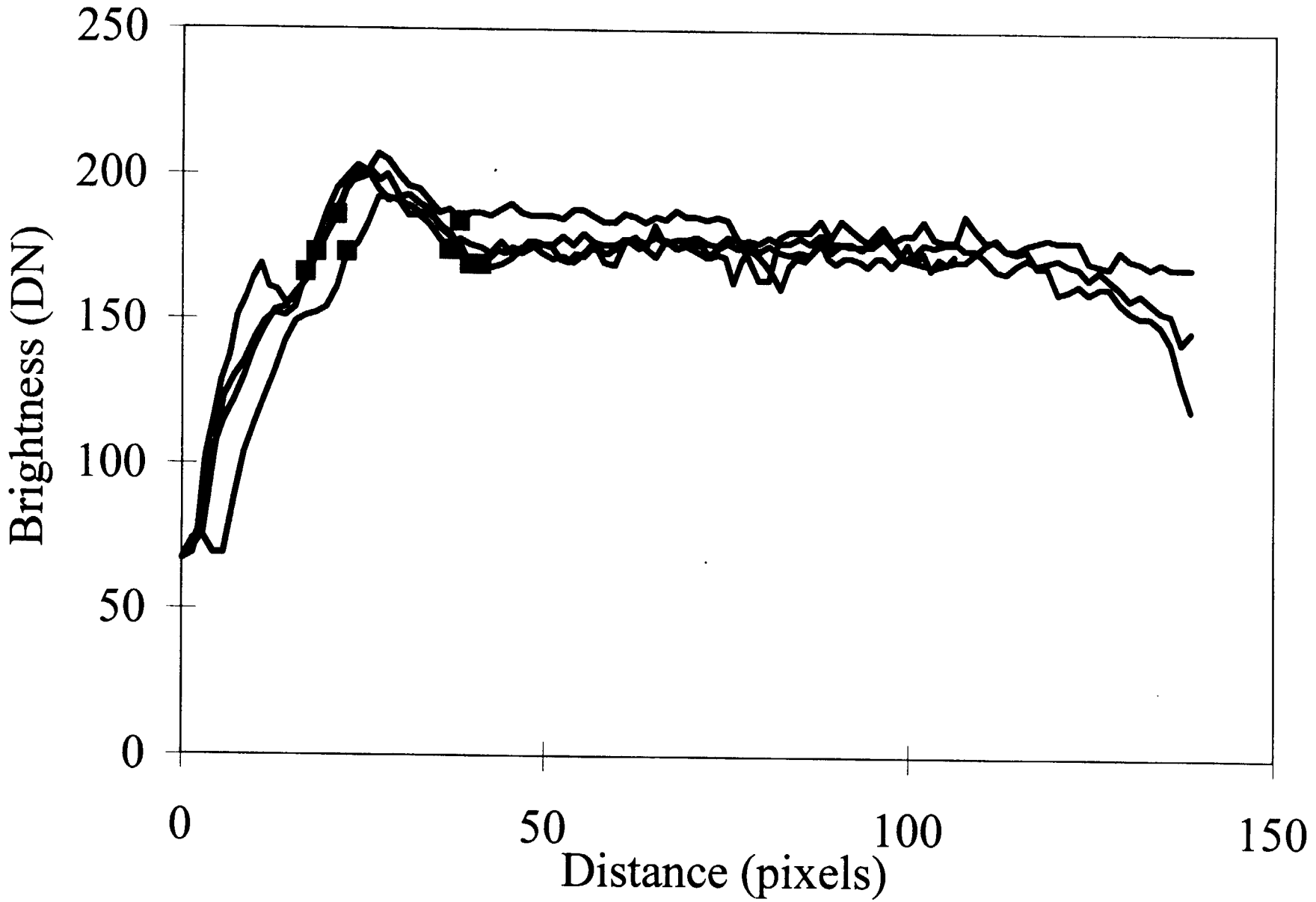
250
200
150
100
50
0
Brightness (DN)
0
50
100
150
Distance (pixels)

Figure 2

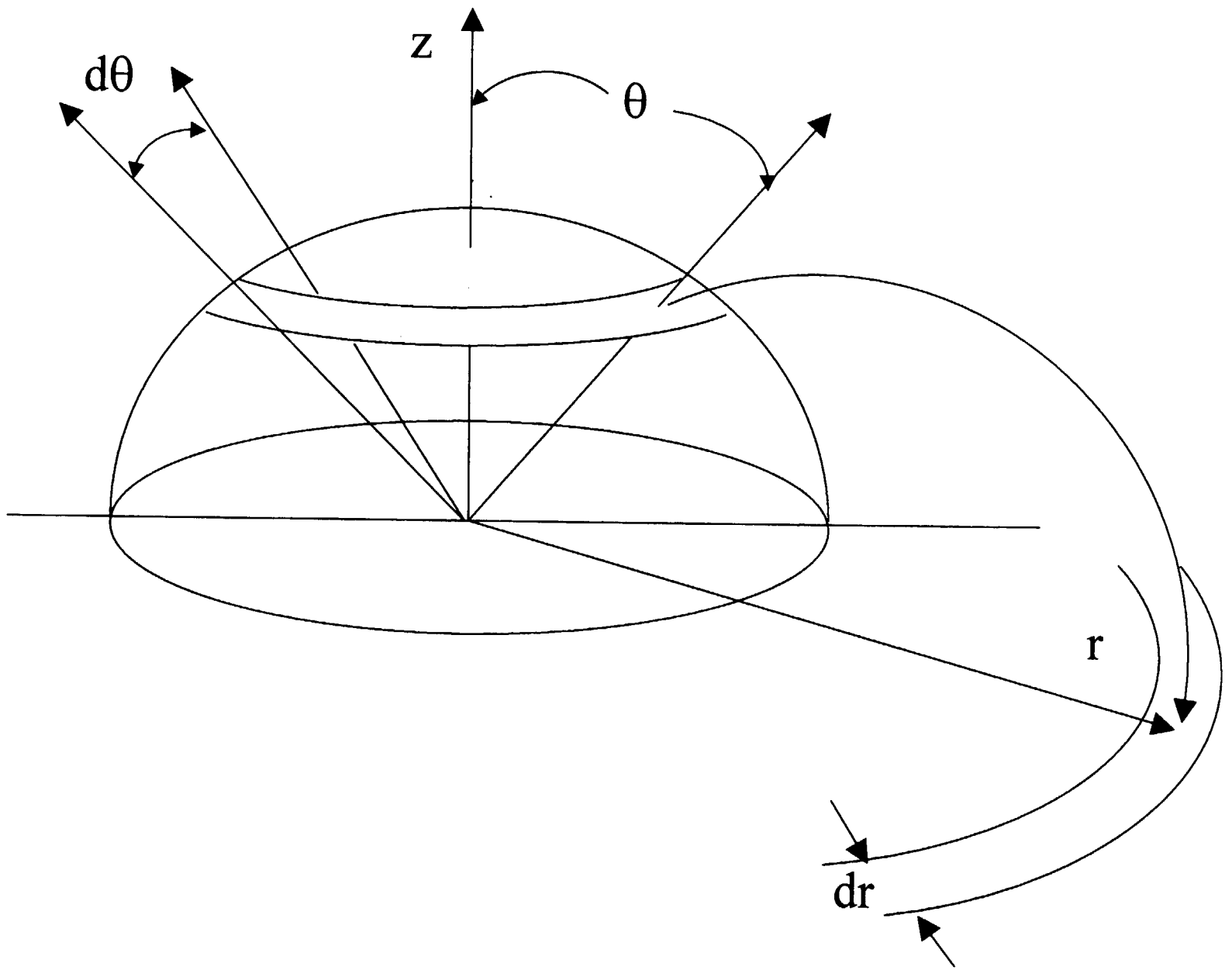

Glaze and Baloga

Figure 3

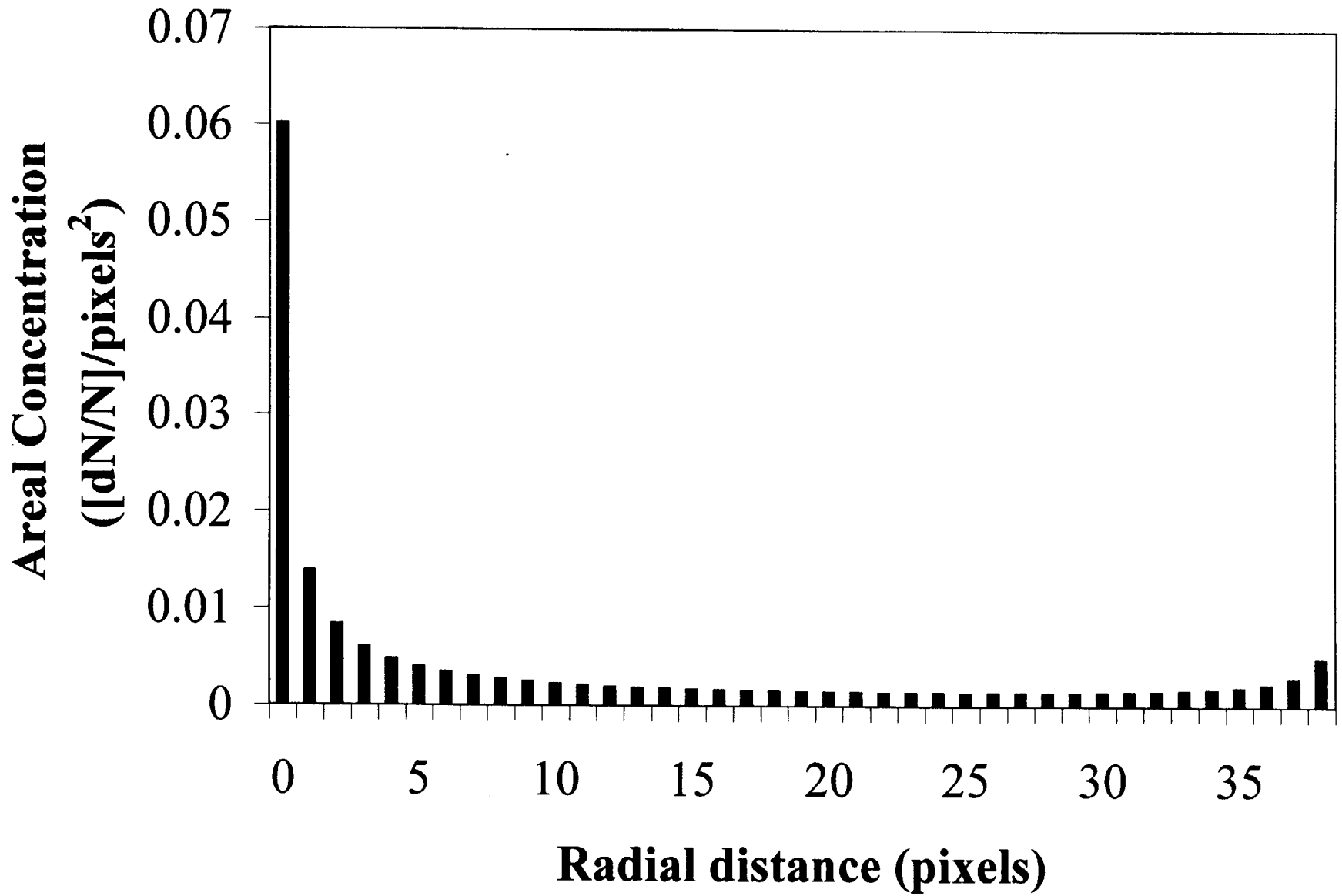
Areal Concentration
([dN/N]/pixels^2)
0.07
0.06
0.05
0.04
0.03
0.02
0.01
0
0
5
10
15
20
25
30
35
Radial distance (pixels)

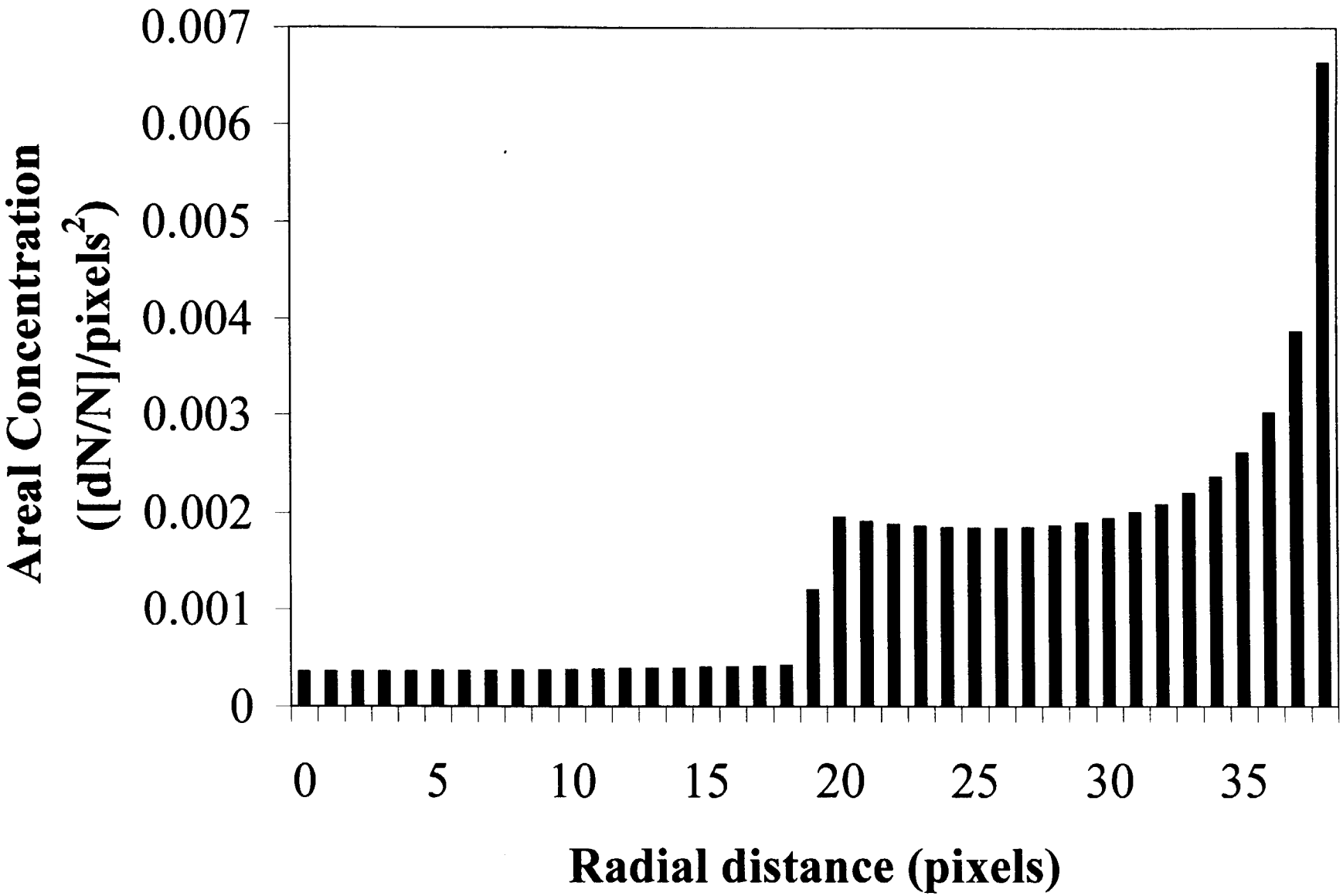
Areal Concentration
([dN/N]/pixels^2)
0.007
0.006
0.005
0.004
0.003
0.002
0.001
0
0
5
10
15
20
25
30
35
Radial distance (pixels)

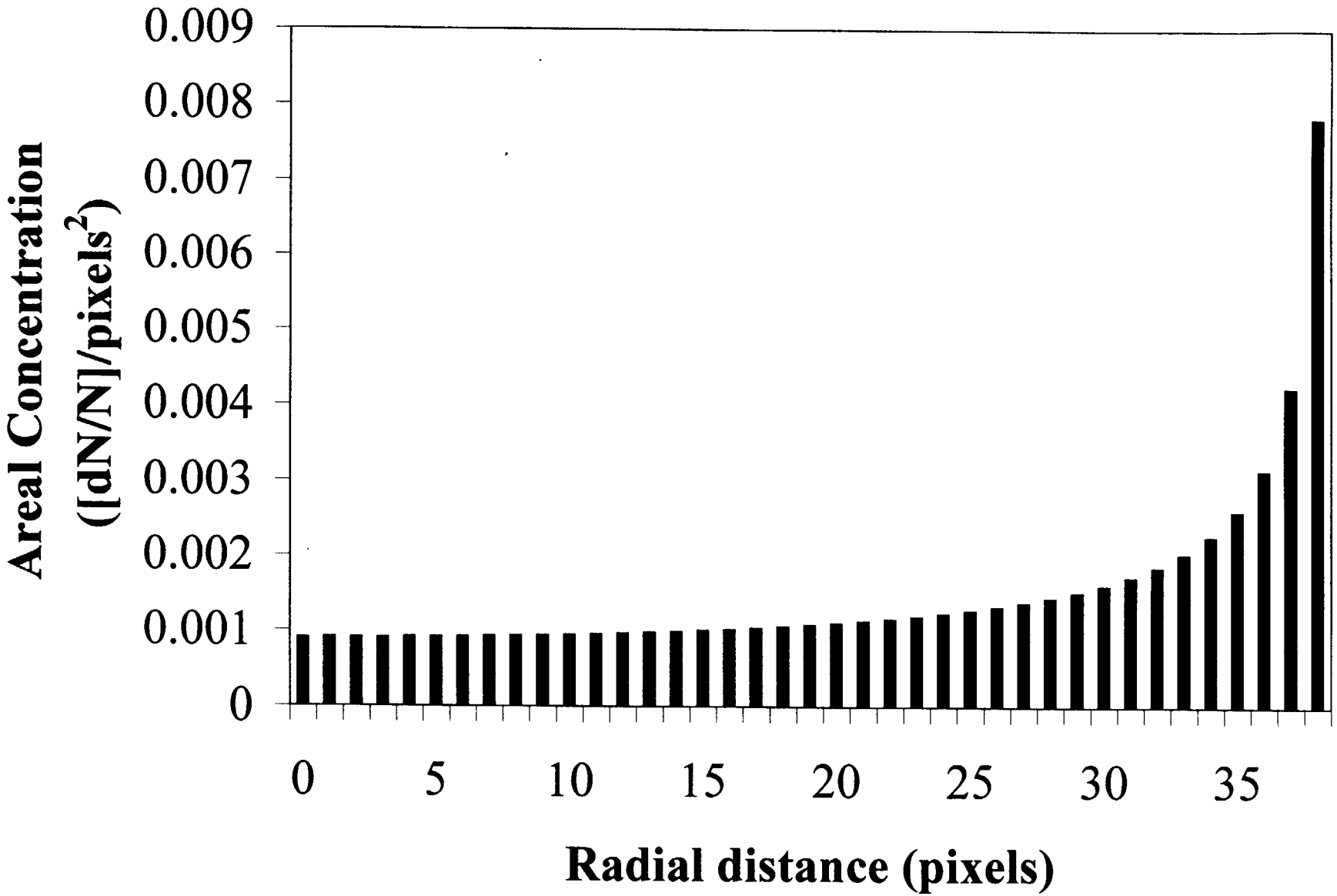
Areal Concentration
([dN/N]/pixels^2)
0.009
0.008
0.007
0.006
0.005
0.004
0.003
0.002
0.001
0
0
5
10
15
20
25
30
35
Radial distance (pixels)

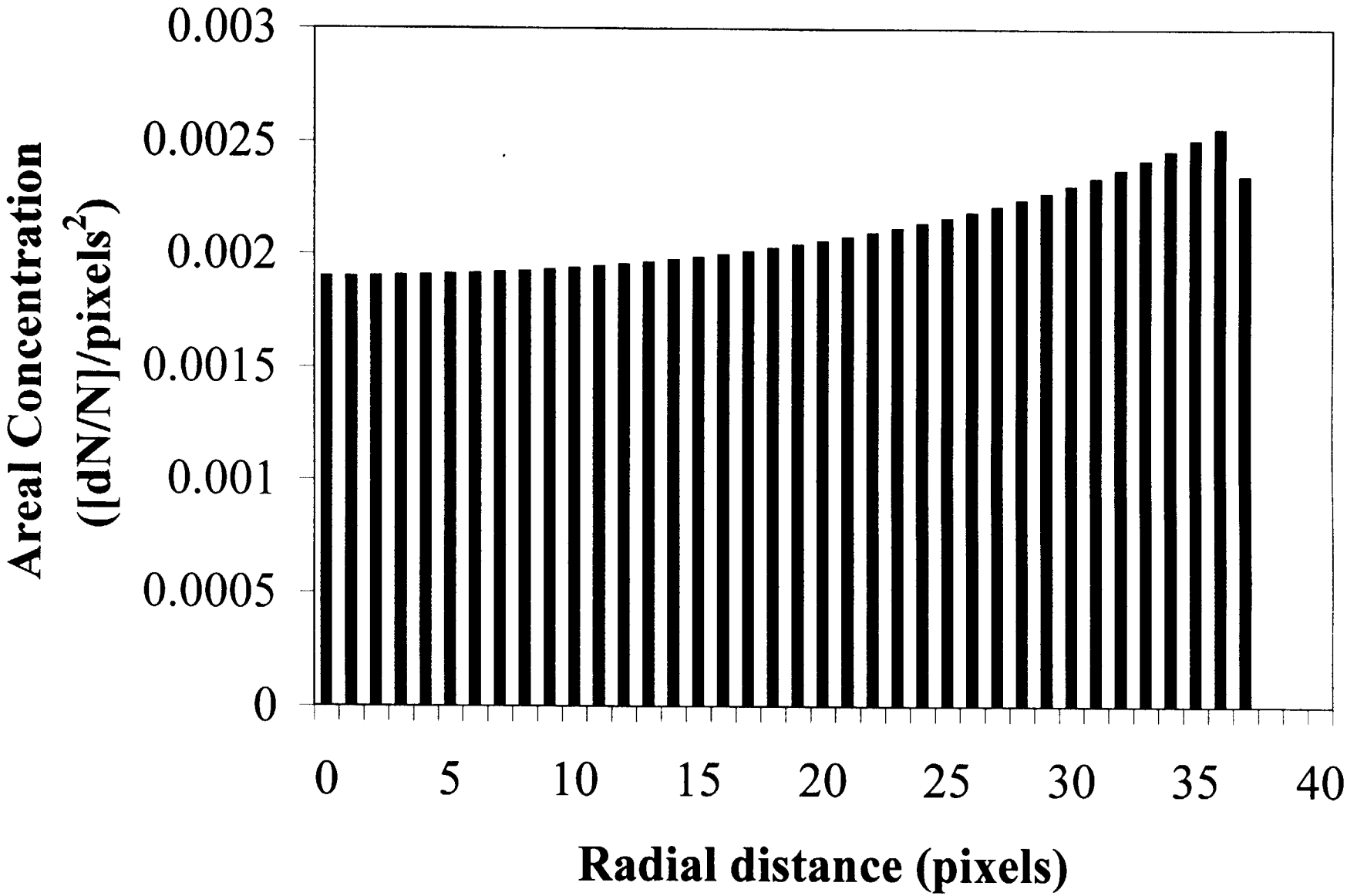
Areal Concentration
([dN/N]/pixels^2)
0.003
0.0025
0.002
0.0015
0.001
0.0005
0
0
5
10
15
20
25
30
35
40
Radial distance (pixels)

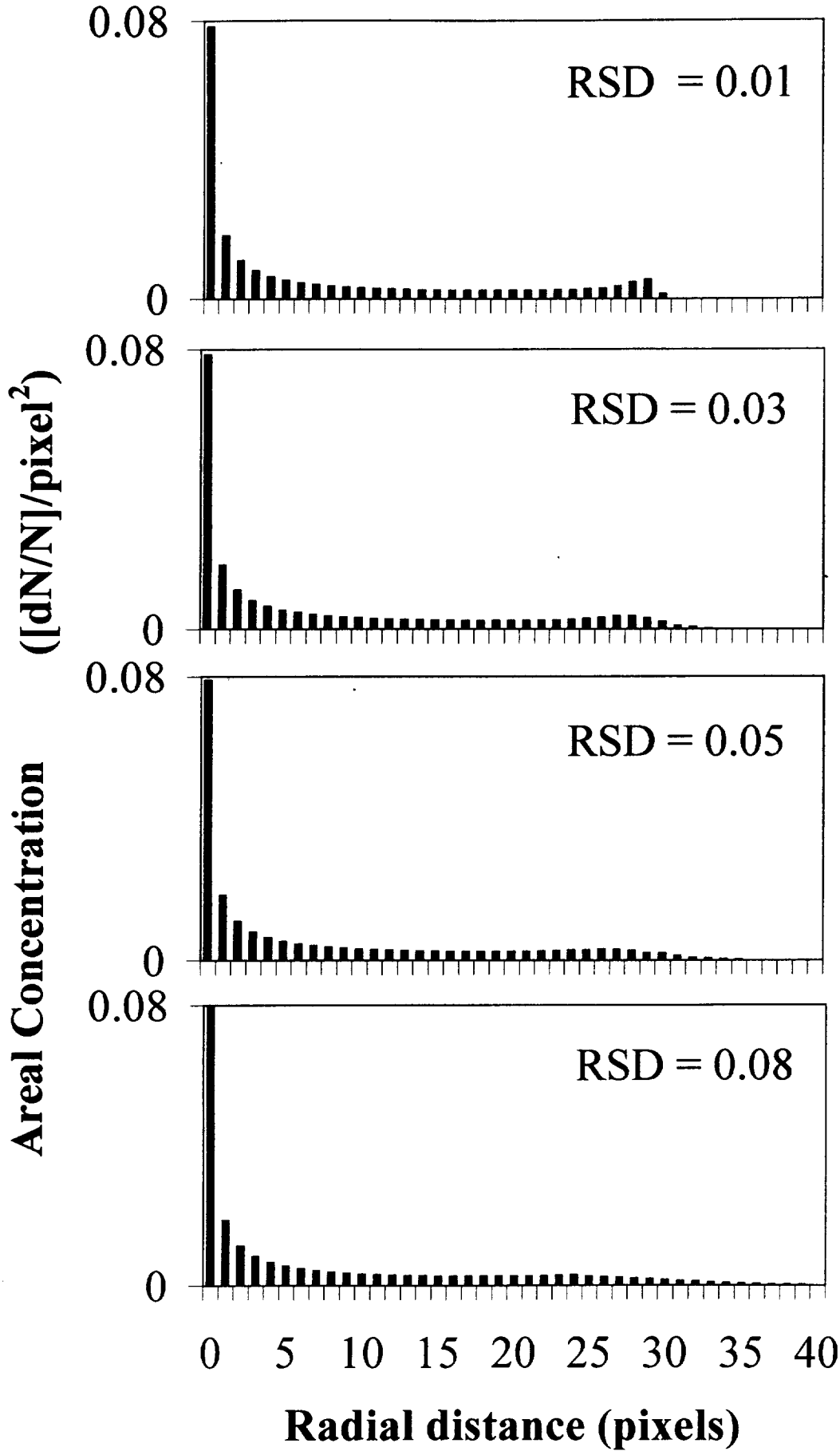

Glaze and Baloga: *Stochastic-ballistic plumes on Io*

Figure 6a

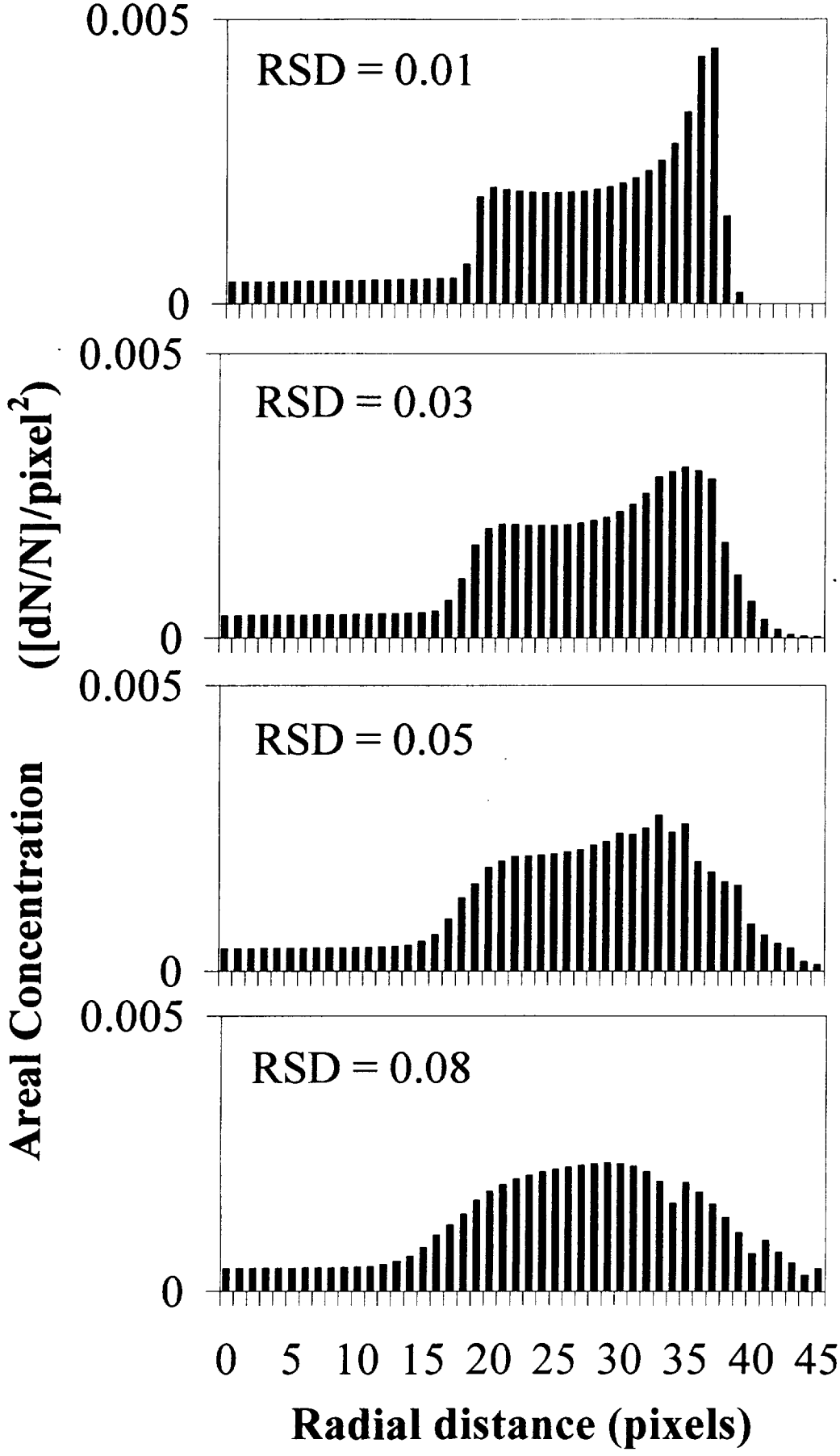

Glaze and Baloga: *Stochastic-ballistic plumes on Io*

Figure 6b

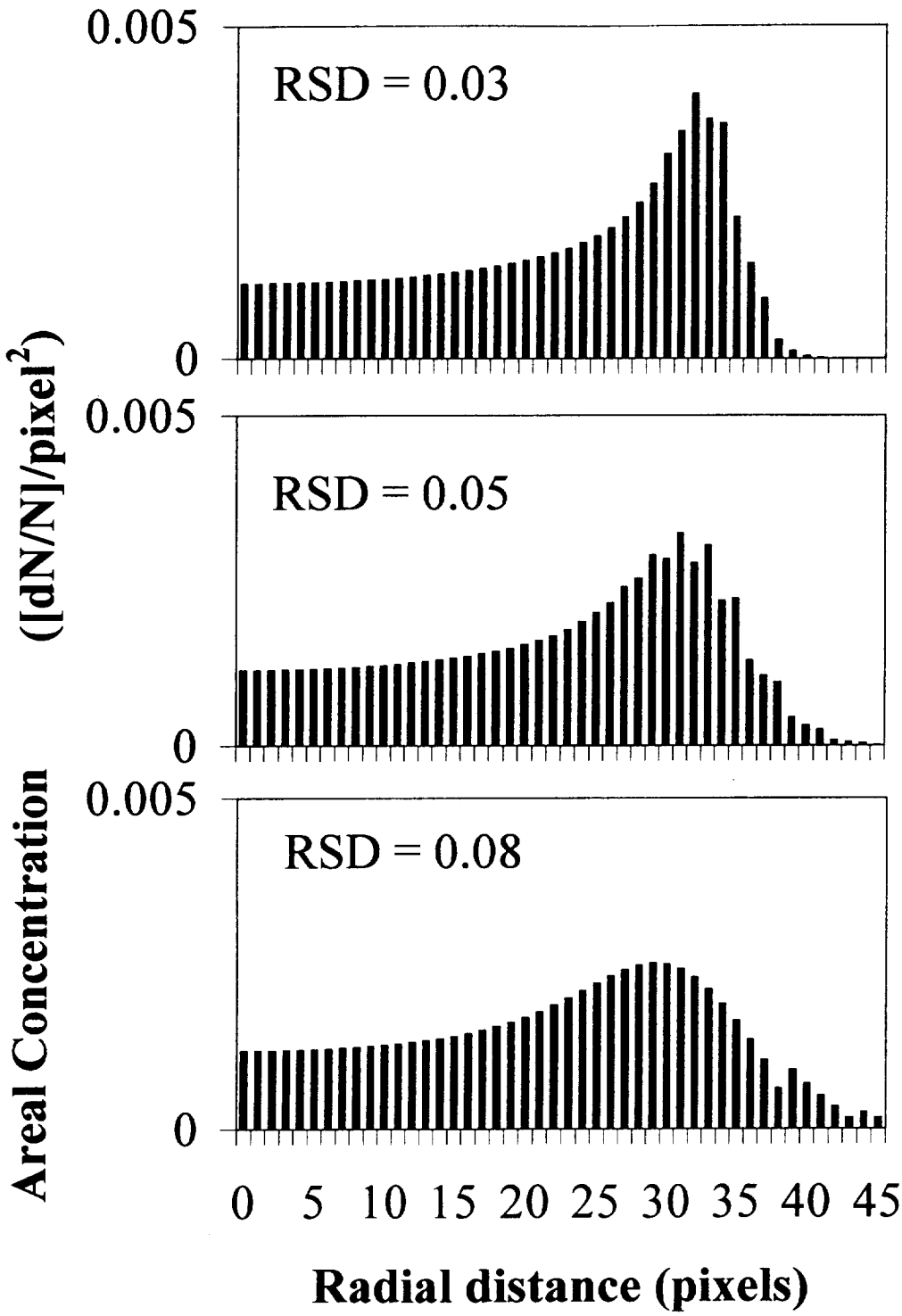
0.005
RSD = 0.03
0
0.005
RSD = 0.05
0
0.005
RSD = 0.08
0
Areal Concentration ([dN/N]/pixel^2)
0 5 10 15 20 25 30 35 40 45
Radial distance (pixels)

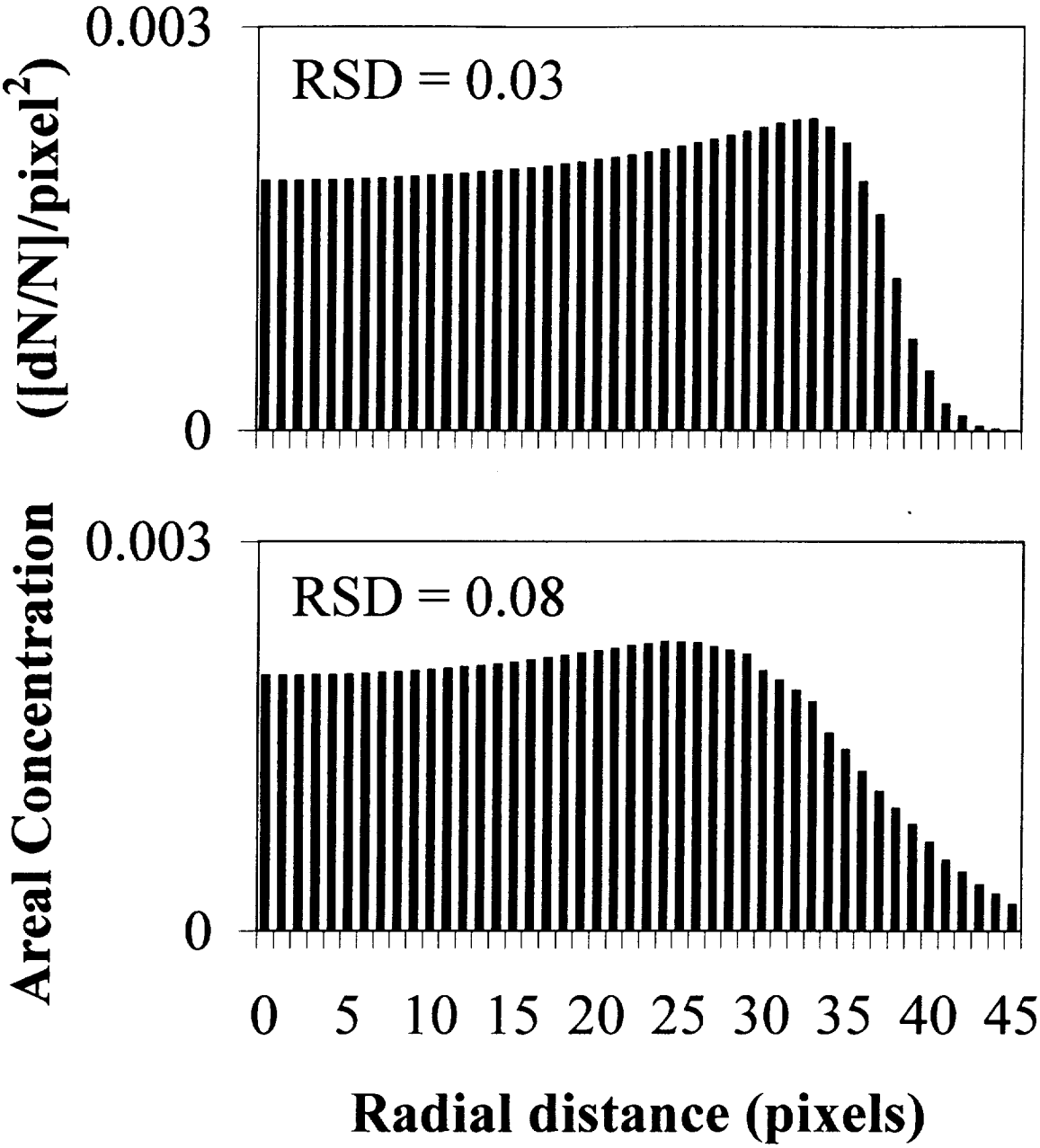
0.003
RSD = 0.03
0
0.003
RSD = 0.08
0
Areal Concentration ([dN/N]/pixel²)
0 5 10 15 20 25 30 35 40 45
Radial distance (pixels)

APPENDIX D:

LPSC Abstract: Stochastic-ballistic plumes on Io

STOCHASTIC-BALLISTIC PLUMES ON IO: SENSITIVITY OF DEPOSITION TO HIGH EJECTION ANGLES. L. S. Glaze and S. M. Baloga, Proxemy Research (20528 Farcroft Lane, Laytonsville, MD 20882, lori@proxemy.com, and steve@proxemy.com).

Introduction: Some active volcanoes on Io are associated with bright annular deposits [1]. These annuli are generally thought to be surface deposits of SO_2 frost [2,3,4]. Glaze and Baloga [5] have extended the plume model developed by Cook et al. [6] to describe the emplacement of particles whose motion is controlled by stochastic processes near the vent and deterministic ballistic transport beyond. Assuming that the relative brightness of the surface deposits observed in visible images is directly related to the areal concentration of particles on the surface, this model now provides quantitative constraints on eruption conditions from the brightness distributions of the annuli.

Random effects within the stochastic region could include particle collisions, thermalization, irregularities in vent conditions and phase changes. The random processes of the stochastic regime are expressed as probability distributions for the important transport variables: energy, momentum, and ejection angles. By varying the parameters of the energy and angular distributions, the stochastic-ballistic model can make annuli of high particle concentrations on the surface come and go.

Choosing a narrow normally distributed ejection energy, instead of a single energy, introduces enough dispersion in the resulting areal concentrations to produce broad annuli with dimensions comparable to those observed at Prometheus [5]. Varying combinations of the truncation angle and relative standard deviation for the energy distribution change the shape and magnitude of the surface deposit.

Glaze and Baloga [5] found that the predicted ground concentrations were very sensitive to high ejection angles (as measured from vertical). This is due primarily to the geometry of hemispherical ejection and a singularity in the areal concentration resulting from ballistic transport. Simple truncation of the ejection cone resulted in a wide range of areal concentrations. Here we explore the effects of allowing a small 'tail' at the outer boundary of the ejection cone on the characteristics of the surface deposits.

The Model: The stochastic-ballistic model used here and in [5] divides a plume into two spatial regions. The stochastic region is considered to be a hemisphere near the vent with a radius that is small compared to the overall dimensions of the plume. In general, we assume that the important transport variables (e.g., energy, momentum, ejection angles) have probability distributions. Once particles leave the stochastic region, the randomizing influences on particle motions cease and the subsequent trajectories are purely ballistic. In effect, the probability distributions are quenched when the plume particles exit the stochastic region. The distributions of transport variables for the stochastic region thus serve as initial conditions for ballistic emplacement.

In this work, we are concerned with the areal concentrations of plume particles on the surface of Io that result from different distributions of transport variables in the stochastic region. We will assume that the plume is axisymmetric and use a cylindrical coordinate system to describe particle trajectories. In the simplest case of ejection of N particles with a single energy, the probability that a particle is ejected at an angle, θ, is

$$P(\theta) = \frac{dN}{N} = C_1 \Theta(\theta) \sin\theta d\theta \qquad (1)$$

where C_1 is the normalization constant and $\Theta(\theta)$ is the angular distribution measured from the vertical axis. For isotropic ejection, $\Theta(\theta) = 1$. The areal concentration on the ground as a function of radial distance, $\rho(r)$, is then given by

$$\rho(r) = \frac{1}{2\pi r}\frac{1}{N}\frac{dN}{dr} \qquad (2)$$

Figure 1 indicates a very high concentration peak near the vent for isotropic ejection out to 90°. The particles forming the peak all originate at angles close to 90° that travel only a short distance from the vent. The high concentration is also a result of the small surface area at that point.

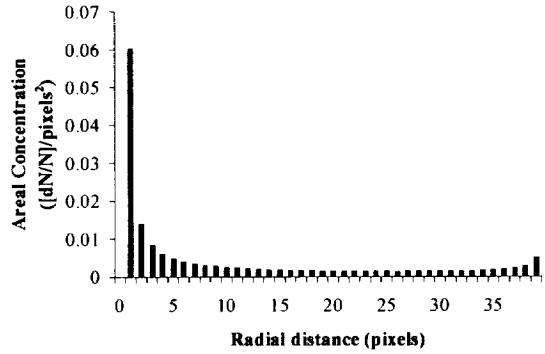

Figure 1. Areal concentration of particles for a single energy and isotropic ejection between 0° and 90°.

Truncating the ejection cone. To examine the sensitivity of the areal surface distribution to the maximum ejection angle, we simply truncate the ejection cone at some angle, θ_o. In general, we will assume that the ejection cone is cutoff at some angle less than 90° and that the distribution is isotropic for $0 \le \theta \le \theta_o$, with relatively few particles ejected beyond θ_o. This approach will allow a small tail in the angular distribution beyond θ_o to some maximum ejection angle.

In the simplest case, no particles are ejected past θ_o. For $\theta_o = 75°$, Figure 2 illustrates how the peak in particle concentration near the vent has been eliminated by cutting off the ejection cone. We see that this results in a broad peak between 20 and 40 pixels from the vent, with a maximum near 40 pixels. Glaze and Baloga [5] have shown that introduction of normally distributed energy with a small relative standard deviation (~8%) results in a broad symmetric peak centered about 30 pixels from the vent that is comparable to the annulus dimensions observed at Prometheus.

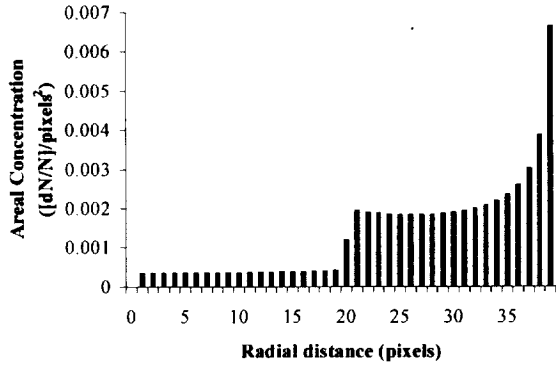

Figure 2. Areal concentration of particles for a single energy and isotropic ejection between 0° and 75°.

The sharp break in the areal concentration (Figure 2) near 20 pixels is a direct result of the cutoff angle. Inside 20 pixels, only the upper plume contributes to the surface deposit. If, however, we allow for a small tail in the angular distribution past the cutoff angle, the surface concentration should have a smoother appearance.

To investigate the influence of a small tail at high ejection angles, we introduce the Fermi function distribution,

$$\Theta(\theta) = \frac{C_2}{1 + e^{(\theta - \theta_o)/\varepsilon}} \qquad (3)$$

where ε is the parameter that controls the sharpness and width of the tail. In the limit as ε goes to 0,

$$\lim_{\varepsilon \Rightarrow 0} \Theta(\theta \le \theta_o) = C_2 \qquad (4)$$

which is simply the isotropic angular distribution up to the maximum ejection angle, and 0 beyond. Otherwise, for finite ε, we need to distinguish between the cutoff angle and the maximum ejection angle. Between these two is the small 'tail' of the angular distribution. The maximum ejection angle is taken to be 90°, the physical limit imposed by the surface.

Normalization of (3) leads to the integral

$$1 = \int_0^{\pi/2} \Theta(\theta) d\theta = C_2 \varepsilon \int_0^{\pi/2} \frac{1}{1+u} \frac{du}{u} \qquad (5)$$

Integrating (5), the normalization constant, C_2, can be found to be

$$C_2 = \left[\frac{\pi}{2} + \varepsilon \ln\left(\frac{1 + e^{-\theta_o/\varepsilon}}{1 + e^{(\pi/2 - \theta_o)/\varepsilon}} \right) \right]^{-1} \qquad (6)$$

Substituting (6) into (3) results in the complete probability function that can replace the previous function given in (1).

Figure 3 shows the Fermi function for several choices of ε. Note that although the probability approaches 0 very quickly beyond θ_o, there is some finite probability of ejection at all angles out to 90°.

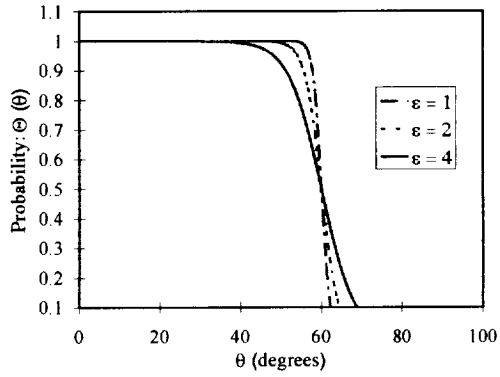

Figure 3. Probability function using Fermi function for ε = 1°, 2° and 4°.

Conclusions: The areal distribution of plume particles on the surface of Io is very sensitive to particles ejected at high angles. Use of the Fermi function, and the limiting process described above, allows us to examine the detailed effects of an ejection cone boundary on annular and other types of areal deposits.

References: [1] A. S. McEwen and L.A. Soderblom (1983) *Icarus 55*, 181-217. [2] T. V. Johnson et al. (1979) *Nature 280*, 746-750. [3] R. G. Strom et al. (1981) *JGR 86*, 8593-8620. [4] A. S. McEwen et al. (1985) *JGR 90*, 12,345-12379. [5] Glaze L. S. and Baloga S. M. (1999) *JGR,*, in review. [6] A. F. Cook et al. (1979) *Nature 280*, 743-746.

REPORT DOCUMENTATION PAGE

Form Approved
OMB No. 0704-0188

1. AGENCY USE ONLY *(Leave blank)*	2. REPORT DATE	3. REPORT TYPE AND DATES COVERED
	30 April 2000	Final Report 1-30 April 00

4. TITLE AND SUBTITLE Interim Progress Report #00-005

5. FUNDING NUMBERS

C NASW-98012

6. AUTHORS Lori S. Glaze

7. PERFORMING ORGANIZATION NAME(S) AND ADDRESS(ES)

Proxemy Research
20528 Farcroft Lane
Laytonsville, MD 20882

8. PERFORMING ORGANIZATION REPORT NUMBER

IO 00-005

9. SPONSORING/MONITORING AGENCY NAME(S) AND ADDRESS(ES)

NASA
Code SR
Washington, D.C. 20546

10. SPONSORING/MONITORING AGENCY REPORT NUMBER

11. SUPPLEMENTARY NOTES

12a. DISTRIBUTION/AVAILABILITY STATEMENT

No limitations

12b. DISTRIBUTION CODE

13. ABSTRACT *(Maximum 200 words)*

Proxemy Research is under contract to NASA to perform science research of volcanic plumes on Venus and Io. This report is submitted in accordance with contract NASW –98012 and contains a summary of activities conducted over the time period indicated in field 3, above. In addition to a synopsis of science research conducted, any manuscripts submitted for publication in this time period are also attached. Abstracts to scientific conferences may also be included if appropriate.

14. SUBJECT TERMS Venus/IO

15. NUMBER OF PAGES
1

16. PRICE CODE

17. SECURITY CLASSIFICATION OF REPORT	18. SECURITY CLASSIFICATION OF THIS PAGE	19. SECURITY CLASSIFICATION OF ABSTRACT	20. LIMITATION OF ABSTRACT
Unclassified	Unclassified	Unclassified	SAR